Structural and metamorphic evolution during tectonic mixing: is the Rocca Canavese Thrust Sheet (Italian Western Alps) a subduction-related mélange?

Manuel Roda[a], Francesca De Salvo[a], Michele Zucali[a], Maria Iole Spalla[a]

[a] *Universita' degli Studi di Milano, Dipartimento di Scienze della Terra, Via Mangiagalli 34, 20133 - Milano (Italy)*

Abstract

In the Sesia-Lanzo Zone (SLZ), the subunit Rocca Canavese Thrust Sheet (RCT) is characterised by a mixture of mantle- and crust-derived lithologies and can be a good candidate to be a former subduction-related mélange of the Austroalpine domain. The unit consists of metapelites, metagranitoids, metabasics, metagabbro and serpentinised lherzolite lenses from metre to hundred-metre size. According to the literature, PT peak conditions for all lithologies are 0.8-1 GPa at 300-400°C, in lawsonite-blueschist facies conditions recorded during the Alpine subduction. However recent work describes different mineral assemblages for the metamorphic peak, separating rocks with lawsonite from those with jadeite. Therefore, we refined the meso and microstructural analysis of the tectonic slices of RCT and we performed a detailed thermo-barometry of different metamorphic stages in order to quantify Alpine peak conditions and P-T-d-t paths, and to test whether the RCT represents a subduction-related mélange. We focus on metagabbros, Jd-bearing and Lws-bearing glaucophanites since they have the most suit-

Email address: manuel.roda@unimi.it ()

able chemistry allowing to reconstruct the complex evolution of the mixing. Metagabbros and Jd-bearing glaucophanites experienced a D1a metamorphic stage characterised by a pressure of 1.3-1.8 GPa and temperature of 450-550°C, in eclogite facies condition. Lws-bearing glaucophanites experienced a D1b metamorphic stage at a temperature <470°C and pressure of ca. 1.2-1.5 GPa, in Lws-blueschist facies condition. The two tectono-metamorphic units (TMUs) were coupled together during the exhumation at D2 stage, under Ep-blueschist facies conditions. Successive evolution occurs at lower pressure, under greenschist facies conditions. D1a peak conditions are compatible with a thermal gradient between a cold and a warm subduction zone while D1b peak is recorded in a thermal gradient compatible with a cold subduction. The coupling between the two TMUs occurred under a cold thermal gradient, suggesting a still active subduction. The different origin and P-T-d-t paths of the blocks, the intense shearing experienced by all lithologies during their coupling and the abundance of serpentinites in the tectonic mixture agree with the interpretation of a subduction-related mélange for RCT, in analogy with other zones of the Alps.

Keywords: Alpine subduction, Austroalpine Domain, multiscale petrostructural analysis, Rocca Canavese Thrust Sheet, tectonic mélange

1. Introduction

Mélanges are rock units characterised both by the lack of internal continuity of contacts or strata and by the inclusion of fragments and blocks of different sizes, lithologies, origin and ages, commonly embedded in a finer-grained matrix (Raymond, 1984; Cowan, 1985; Cloos & Shreve, 1988; Polino

et alii, 1990; Festa *et alii*, 2010; Dilek *et alii*, 2012; Balestro *et alii*, 2015; Wakabayashi, 2015; Ernst, 2016). The criteria of matrix composition and fabric are not employed in the definition of the term mélanges (Raymond, 1984). Mélanges may be subdivided into tectonic, diapiric, allolistostromes, and polygenetic mélanges where the primary cause of fragmentation and mixing is known to be tectonic, diapiric, sedimentary, or a combination of processes, respectively (Raymond, 1984).

Although tectonic mélanges may characterize different geodynamic environments of formation, they are commonly associated with subduction of oceanic lithosphere and collisional events, and originate in an accretionary wedge or in a subduction channel during subduction-exhumation processes (Festa *et alii*, 2010; Dilek *et alii*, 2012). In these environments, a tectonic mixing of relatively poorly deformed lenses (from m- to km-scale) of heterogeneous lithologies with contrasting P-T-d-t paths, enclosed in highly sheared serpentinite and/or metasediments rocks, occurs (Gerya & Stöckhert, 2005; Federico *et alii*, 2007; Guillot *et alii*, 2009; Roda *et alii*, 2010; Malatesta *et alii*, 2012; Roda *et alii*, 2012; Wakabayashi, 2015; Ernst, 2016).

Examples of subduction-related tectonic mélanges have been widely reported from the Alps (e.g. Polino *et alii*, 1990; Spalla *et alii*, 1996; Festa *et alii*, 2010; Ernst, 2016) from East (e.g. Frisch, 1984; Ring *et alii*, 1988; Winkler, 1988) to West (Caron *et alii*, 1989; Schwartz, 2000; Balestro *et alii*, 2015; Tartarotti *et alii*, 2017). For example, in the Voltri Massif tectonic mélange (Penninic domain of Western Alps), a schistose chlorite-actinolite matrix encloses metre-scale blocks of metagabbros,

metabasites, metasediments and serpentinites (Federico *et alii*, 2007). The massif underwent a polyphase deformation before and after the tectonic mixing occurred in a serpentinite-subduction channel (Malatesta *et alii*, 2012). A similar interpretation has been proposed for the Furgg zone (Penninic domain of Western Alps) on the basis of its chaotic character and heterogeneous composition, including continental basement rocks, serpentinite, and Permian Mesozoic continental cover (Milnes *et alii*, 1981; Froitzheim, 2001). The Arosa zone (Penninic domain of Central-Eastern Alps) is characterised by a tectonic mélange of blocks of both Austroalpine and Penninic origin embedded in a serpentinitic or shaly-calcareous matrix (Ring *et alii*, 1990). Finally, the Adula-Cima Lunga nappe (Penninic domain of Central Alps) consists of a mixture of mafic and ultramafic rocks surrounded by pelitic-gneiss of pre-Alpine basement (Jenny *et alii*, 1923). This mixture of rocks within a narrow zone is best interpreted as a tectonic mélange formed in a subduction zone (Trommsdorff, 1990). More recent investigations on the Adula nappe, suggest that its rocks were subducted and exhumed together during the Alpine convergence (Herwartz *et alii*, 2011; Cavargna-Sani *et alii*, 2014; Sandmann *et alii*, 2014). Unfortunately, these contributions lack of a detailed structural analysis correlating the Alpine tectonic history with the polyphase metamorphic evolution. The assemblage of units consisting of highly deformed and imbricated slices of pre-Alpine continental crust and mantle, elongated parallel to the Southern Steep Belt of the Central Alps and characterized by variable metamorphic grade, has been interpreted as a tectonic mélange formed in a subduction channel (Engi *et alii*, 2001, 2004).

In the rocks of the Austroalpine domain of the Western Alps different PT

conditions and P-T-d-t paths are recorded during the Alpine subduction and their exhumation is generally achieved in a cold thermal state compatible with a still active subduction (Spalla *et alii*, 1996, 2010; Stöckhert & Gerya, 2005; Bousquet, 2008; Meda *et alii*, 2010; Roda *et alii*, 2010, 2012). For this reason, the Sesia-Lanzo Zone (SLZ) has been interpreted as a tectonic mixture of mainly continent-derived rocks (e.g. monometamorphic metasediments, pre-Alpine marbles, granulites and amphibolites, Permian granitoids, partly serpentinized peridotites), originated in a subduction channel (Pognante, 1989a; Ferraris & Compagnoni, 2003; Spalla & Zulbati, 2003; Gerya & Stöckhert, 2005; Meda *et alii*, 2010; Roda *et alii*, 2012). In the southern part of the Sesia-Lanzo Zone (SLZ), the Rocca Canavese Thrust Sheet (RCT) is characterised by mixing of mantle and crust-derived lithologies (Pognante, 1989a; Spalla & Zulbati, 2003; Barnes *et alii*, 2014; Cantù *et alii*, 2016), and may be interpreted as a former subduction-related mélange of the Austroalpine domain.

Pognante (1989a) indicates similar PT peak conditions in all lithologies at 0.8-1 GPa and 300-400°C, in the lawsonite stability field, during the Alpine subduction, and this would contrast with the requirement of different P-T-d-t paths recorded in the blocks of a subduction-related mélange. However, in a recent structural map of the RCT, Cantù *et alii* (2016) describe different mineral assemblages developed under peak conditions, characterised by lawsonite or jadeite respectively. Such assemblage differences suggest the possible occurrence of different metamorphic evolutions, which must be checked with the reconstruction of quantitative P-T-d-t paths that have not been inferred so far. With this purpose, the meso and microstructural analysis of the

tectonic slices of RCT has been refined and micro-structurally constrained thermo-barometric estimates have been performed in metabasites in order to quantify Alpine P-T-d-t paths. Such tests help to evaluate whether the tectonic mixture can be interpreted as a tectonic mélange.

2. Geological Setting

The RCT is the most internal portion of the SLZ (Fig. 1), the widest Austroalpine nappe of the Italian Western Alps. The SLZ predominantly consists of Palaeozoic continental basement rocks (Compagnoni, 1977) characterised by pre-Alpine amphibolite to granulite facies metamorphism which occurred during Permian extension-related uplift (Lardeaux & Spalla, 1991; Rebay & Spalla, 2001; Schuster & Stüwe, 2008; Spalla *et alii*, 2014). The alpine evolution is characterised by polyphase deformation under blueschist to eclogite facies conditions followed by retrogression under blueschist to successive greenschist facies conditions (Gosso, 1977; Pognante *et alii*, 1980; Lardeaux *et alii*, 1982; Williams & Compagnoni, 1983; Vuichard, 1987; Spalla *et alii*, 1991, 1996; Zucali *et alii*, 2002; Gosso *et alii*, 2010; Zucali, 2011; Zucali & Spalla, 2011) variably recorded by the different metamorphic complexes. Alpine metamorphism occurred under low T/depth ratio (ca. 6°C/km), compatible with cold subductions (Cloos, 1993; Handy & Oberhänsli, 2004; Meda *et alii*, 2010; Roda *et alii*, 2012), which persisted until the exhumation of the SLZ, as testified by blueschist-facies re-equilibration (Spalla *et alii*, 1996; Zucali *et alii*, 2004; Zanoni *et alii*, 2010). This led to the interpretation of exhumation process accomplished during ongoing active oceanic subduction (Zucali

et alii, 2004; Stöckhert & Gerya, 2005; Berger & Bousquet, 2008; Zanoni *et alii*, 2008; Meda *et alii*, 2010; Roda *et alii*, 2012).

The SLZ is traditionally subdivided into different elements (e.g. Dal Piaz *et alii*, 1972; Compagnoni, 1977; Spalla *et alii*, 1983; Pognante, 1989a; Stünitz, 1989; Spalla *et alii*, 1991; Wheeler & Butler, 1993; Handy & Oberhänsli, 2004; Babist *et alii*, 2006; Manzotti *et alii*, 2014; Cantù *et alii*, 2016). The Seconda Zona Diorito-Kinzigitica (IIDK), comprises metapelites and metabasics of the lower crust that do not record the Alpine eclogitic re-equilibration. The second element consists of polymetamorphic metapelites, metagranitoids, metabasics and marbles, from the lower and upper crust, intruded by Permian igneous bodies (e.g. Oberhänsli *et alii*, 1985; Rebay & Spalla, 2001; Zucali *et alii*, 2002) and it is further divided into two metamorphic complexes: the Gneiss Minuti (GMC) and the Eclogitic Micaschists (EMC), both pervasively eclogitized during the Alpine event but with different rock-volume recording greenschist-facies re-equilibration (Stünitz, 1989; Spalla *et alii*, 1991; Gosso *et alii*, 2015; Corti *et alii*, 2017).

The RCT has been recognized as a further metamorphic complex belonging to the SLZ (Pognante, 1989a) and consists of juxtaposed thrust sheets derived from pre-alpine continental crust and upper mantle (Pognante, 1989a,b; Spalla & Zulbati, 2003; Barnes *et alii*, 2014). Such tectonic slivers are limited by blueschist/greenschist-facies mylonitic zones of Alpine age and are bounded by the EMC to the Northwest, the Southalpine domain eastward, on the other side of the Periadriatic (Canavese) Lineament, and the Lanzo Massif (LM) southward (Fig. 1). The latter is an ultramafic complex

made up by mantle peridotites that were exhumed during lithospheric extension related to the formation of the Ligurian oceanic basin (158-163 Ma, e.g. Pognante *et alii*, 1985; Müntener *et alii*, 2005; Piccardo, 2010; Guarnieri *et alii*, 2012; Rampone *et alii*, 2014) and involved in Alpine convergent tectonics (Pelletier & Müntener, 2006; Scambelluri *et alii*, 2017).

3. Lithologies and mesostructural features

One of the most striking features of the RCT is the intimate mixing between mantle- and crust-derived lithologies, which locally occurs at metric scale (Cantù *et alii*, 2016, Figs 2, 3 and 4). The unit consists of metapelites, metagranite, metabasics, metagabbro and serpentinised lherzolite lenses from metre to hundred-metre size (Spalla & Zulbati, 2003; Cantù *et alii*, 2016, Fig. 4a,b).

Metapelites crop out in the central-western sector, toward the EMC contact (Figs 1 and 2), and consist of paragneisses and micaschists characterised by alternation of quartz, plagioclase, epidote-rich layers and blue-green amphibole, white mica and chlorite-rich layers. Locally, quartz-rich alternate with jadeite, white mica and garnet-rich layers (Cantù *et alii*, 2016); metagranitoids are less frequent and crop out in the eastern part of the RCT. They are characterised by fine-grained blue amphibole, white mica-rich and quartz and K-feldspar-rich alternating layers (Cantù *et alii*, 2016). Metabasics consist of glaucophanites and metagabbros and minor pyroxenites and omphacitites; they may be derived from oceanic or continental protoliths (Cantù, 2011). Glaucophanites crop out in the central portion of the RCT

and some lenses can be locally found in the surrounding micaschists. Glaucophanites have a tectonitic to mylonitic fabric and consist of glaucophane, epidote, white mica, quartz, titanite and minor rutile, garnet, albite, chlorite, actinolitic amphibole, stilpnomelane and green biotite. Lawsonite- and pumpellite-bearing glaucophanites crop out mainly at the contact with the Mylonitic Zone (Fig. 2), separating the RCT from the EMC and the LM. Few metagabbro lenses are enclosed in glaucophanites and serpentinites and are characterised by coronitic to mylonitic fabric with porphyroclasts of clinopyroxene and fine-grained aggregate of white mica, epidote, and locally preserving the omphacite-garnet association (Cantù *et alii*, 2016). Serpentinites outcrop in the central and eastern part of the RCT and are generally thinly foliated, with serpentine SPO marking foliation planes. They locally contain metre- to decimetre-sized lenses preserving pyroxene and rare spinel (Cantù *et alii*, 2016).

Multi-scale structural studies performed on the southern portion of the RCT led to the recognition of four groups of structures (Pognante, 1989a,b; Spalla & Zulbati, 2003) and the following description is a synthesis of the work of Cantù *et alii* (2016), which also contains details on fabric element orientations. Mineral abbreviations are according to Whitney & Evans (2010). Mineral associations characterising the dominant fabrics are summarized in Table 1. The first group of structures (D1) mainly consists of the S1 foliation, preserved in metapelites and marked by the SPO of Wm, Amp and Qz. S1 is locally mylonitic and in these cases is defined by fine-grained Jd, Wm, Ep and Qz-rich layers wrapping Grt, Jd and Ep porphyroclasts. In the metagabbros and glaucophanites the oldest metamorphic relicts are

Omp and Grt (D1a) or Gln, Grt and Lws (D1b).

D2 developed under blueschist-facies condition and is responsible for the transposition of the original lithostratigraphy, as demonstrated by gabbro boudins within the serpentinites and by glaucophanite lenses within metapelites. S2 fabric, associated to the D2 stage, is the most pervasive structure in metapelites, metagranitoids and glaucophanites (Fig. 4a, b, c, d), and is mylonitic and defined by compositional layering and SPO of Gln, Wm, Pl and Ep. In metagabbros D2 is mostly characterised by discontinuous S2 foliation marked by SPO of Gln, Wm, Ep and Grt (Fig. 4e, f). In serpentinites S2 is mylonitic and marked by SPO of Srp and Opq trails. S2 foliation planes describe a main cluster dipping to the NE at approximately 30 degrees.

D3 stage developed under greenschist-facies conditions and consists of a centimetre to metre-scale folding (PA3), associated with S3 axial plane foliation with a main vertical NE striking orientation (Fig. 4b, c). The S3 foliation is commonly marked by the SPO of Wm, green Amp, Chl and Ep in crustal rocks and by SPO of Srp in serpentinites. D4-related structures still developed under greenschist-facies conditions, and are recorded only in metapelites. D4 consists of a centimetre-spaced crenulation, locally associated with a rough cleavage, marked by SPO of Chl and Wm.

The tectonic contact between the RCT, the EMC and the LM is characterised by a 100-200-metre-thick mylonitic zone that develops between the EMC and the RCT to the North and the LM and the RCT to the South (Figs 1, 2 and 3); the mylonitic zone started forming during D2, under blueschist-facies conditions (Spalla & Zulbati, 2003; Cantù *et alii*, 2016). It com-

prises the same rocks forming the RCT with the addition of silicate-bearing marble and was active from blueschist- (D2) to greenschist- (D3) facies conditions, associated with the occurrence of km-scale asymmetric folding (PA3) affecting the contact between RCT and EMC.

4. Microstructural analysis

Although several rock associations characterise the RCT, we focus our analysis on two main lithologies, namely metagabbros and glaucophanites. On the basis of Jd and Lws occurrence, the glaucophanites are further divided in Jd- and Lws-bearing glaucophanites. Within the three rock types, four main groups of superposed meso and microstructures may be separated on the basis of their geometrical and kinematic coherence and mineral associations (Table 2). Same mineral phases growing at different stages are numbered progressively, starting from their first occurrence in the rock. Minerals stable through different stages keep the same number.

4.1. Stage M0 - Magmatic event

The oldest event is represented by igneous mineral relics with granular texture, preserved within coronitic metagabbros, such as Cpx1 and rare Opx1, with interlobate margins towards ex-Pl sites totally replaced by microaggregates (Fig. 5a). Cpx1 grains are generally subhedral and highly deformed, showing undulose extinction, kink bands and mechanical twins. Cpx1 porphyroclasts are frequently fractured, sometimes with microboudinage and domino microstructures. Cpx1 grain-boundaries are often replaced by Amp fibres or by a fine-grained aggregate of Chl, Ep and Opq (Fig. 5b). Ex-Pl

sites are represented by aggregates alternatively of Pmp, Chl, Ep and Wm or Wm only.

4.2. Stage M1a/D1a

M1a/D1a is the oldest metamorphic stage preserved in these rocks and is recorded only in metagabbros and Jd-bearing glaucophanites. In metagabbros M1a corresponds to coronitic blastesis of Cpx2 and Grt1 in ex-Pl sites. Cpx2 also occurs as exolutions in Cpx1 porphyroclasts or as coronas on Cpx1 (Fig. 4b, c, d).

In the Jd-bearing glaucophanites D1a is associated with Jd1, Wm1, Grt1 and Ep1 growth. Jd1 granoblastic aggregates constitute 1-2 mm-sized sites with brownish colour at plane polarized light (Fig. 6a), or occur as Jd1+Qz symplectites. Wm1 is rare and generally associated to Jd1+Qz domains, together with Grt1. Grt1 and Ep1 occur as fine-grained (0.5 mm) subhedral porphyroclasts wrapped by the main foliation (S2). Few subhedral Ttn porphyroclasts occur in fine-grained portions and are wrapped by the S2 foliation.

Therefore, the assemblages interpreted as stable during stage pre-D2a are (Table 2) Cpx2+Grt1 in metagabbros and Jd1+Wm1+Grt1+Ep1±Ttn±Qz in Jd-bearing glaucophanites.

4.3. Stage D1b

D1b stage is recorded in Lws-bearing glaucophanites only and is marked by medium size Gln1, Wm1, Grt1, Lws1 and Ep1 porphyroclasts wrapped by S2 tectonitic to mylonitic foliation (Fig. 7a, b). Gln1 is the most abundant

phase in these samples. It is generally well preserved and forms millimetre-size euhedral crystals. It is present both in microlithons, where it is generally randomly oriented, and in films progressively parallelised to foliation direction (S2) toward cleavage domains (Fig. 7a, b, c). Gln1 is often associated with Wm1 along foliation planes or as S1 relict in D2 fold hinges (Fig. 7a, b); in both cases they form rational grain boundaries. Some Gln1 grains are zoned and locally they show undulose extinction. Grt1 occurs as millimetre-size euhedral porphyroclasts dismembered by micro-boudinage and wrapped by S2. Lws1 occurs in low D2 strain domains with SPO aligned in S1 (Fig. 7d, e, f). Lws1 relicts are also found within Grt1 porphyroclasts. Lws1 crystals contain deformation lamellae. Ep1 constitutes submillimetre-size subhedral porphyroclasts wrapped by S2 foliation. Ep1 is locally micro-boudinaged and Ep2 crystals occur in the necks, aligned toward foliation direction. Ttn porphyroclasts are sited in finer grained portions and are wrapped by S2.

Therefore, the assemblages interpreted as stable during stage pre-D2b in Lws-bearing glaucophanites are Gln1+Wm1+Grt1+Lws1+Ep1±Ttn±Qz.

4.4. Stage D2

All rocks experienced D2 deformation, which is responsible for the most pervasive foliation in all rocks. In metagabbros D2 is associated with blastesis of Gln1 and Wm1 on Cpx1 and by Grt2 in association with Gln1 in coronas around Cpx1 porphyroclasts. Tectonitic and mylonitic metagabbros are characterised by lenticular polycrystalline domains elongated within S2. Gln1 mainly occurs in medium sized anhedral crystals replacing Cpx2, with SPO parallel to S2. Grt2 mainly occurs in coronas around Cpx1 porphyroclasts, usually associated with Gln1, Ep1 and Chl1. Wm1 usually shows

SPO, sometimes LPO, parallel to Cpx2 cleavages or internal foliation. Wm1 is very fine-grained and intergrown with Chl1. Ep1 generally constitutes millimetre-sized aggregates together with Chl1, Gln1 and Wm1 in interstitial domains between Cpx1 and Cpx2 porphyroclasts. Ep1 is locally arranged with an SPO that defines an incipient foliation and occurs in S2 microlithons. Ep1 has also been detected in Cpx1 and Cpx2 coronas. Micro-boudinage of some Ep1 grains occurs. Chl1 develops without any preferred orientation in interstitial domains between Cpx1 and Cpx2 or occurs in association with Ep1 and Wm1. Pmp1 usually occurs in interstitial domains between Cpx1 and Cpx2 and is generally well-preserved with euhedral habitus (Fig. 5c, d), showing rational grain boundaries with Ep1.

In Jd-bearing glaucophanites S2 foliation is marked by elongated Jd1 porphyroclasts surrounded by medium grained Gln1 and Grt2 rich layers (Fig. 6c, d, e). Locally Gln1 occurs inside Jd1+Qz+Grt1 domains (Fig. 6f). Layered microcrystalline matrix of Ep2 and Pl wraps Ttn and Ep1. Ep2 crystals can be also found in Gln1- and Grt2-rich layers.

In Lws-bearing glaucophanites S2 foliation ranges from spaced to continuous and is marked by SPO and LPO of Wm1 and SPO of Gln2, associated with fine-grained Ep2, Ttn and Qz and, locally, isoriented Pmp1 crystals. Cleavage domains wrap Grt1, Ep1 and Lws1 porphyroclasts. Grt1 is micro-boudinaged during S2 development. Gln2 is found in cleavage domains and has SPO parallel to S2. Recrystallised fine-grained Ep2 forms monomineralic microlithons. Locally, Ep2 occurs within boudin necks of Ep1, elongated in S2. Grt2 grains are in round-shaped sites wrapped by S2 films; such round-shaped sites are replaced by randomly oriented Chl. Rare Pmp is fine-grained

and subhedral and occurs in grains parallel or at high angle to S2 and locally replacing Lws1. These ambiguous deformation-blastesis relationships make the timing of growth of Pmp doubtful (late-D2 or M3).

Therefore, the assemblages interpreted as stable during stage D2 are

Gln1+Grt2+Wm1+Ep1±Pmp1±Chl1 in metagabbros,

Gln1+Grt2+Ep2±Chl1±Pl±Wm1±Qz±Opq in Jd-bearing glaucophanites and

Gln2+Grt2+Wm1+Qz±Ep2±Pmp1±Ttn±Opq in Lws-bearing glaucophanites.

4.5. Stage D3

D3 deformation is recorded in metagabbros and Lws-bearing glaucophanites, with various degrees of fabric evolution (e.g. Salvi *et alii*, 2010), generally characterised by a discontinuous S3 foliation, locally re-activating S2. In metagabbros stage D3 is characterised by re-crystallisation of S2 minerals into fine-grained aggregates and growth of green Amp1, Grt3, Chl2, Wm2 and Ep2. Green Amp1 is small-sized and subhedral. Chl2 shows SPO and LPO parallel to S3. Some Pmp1 grains are micro-boudinaged and Chl2 and green Amp1 fibres fill the boudin necks. Locally Pmp2 develops in association with Chl and fine-grained Ep2. Grt3 develops along Grt1/2 grain boundaries or locally replaces Grt1/2 cores, or fills veins in coronitic metagabbros, but no diagnostic relationships with S3 or S2 have been observed. Consequently their growth is attributed to M3 stage, postdating syn-D2 Grt-growth.

In Lws-bearing glaucophanites D3 is associated to partial replacement of Gln2 and Wm1 by green Amp1, Chl1 and green Bt1 along grain boundaries and fractures, mimetic growth of Chl1 on S2 or pseudomorphic replacement

of Chl1 on Grt1. Pmp2 in association with Chl1 and Ep3 constitutes micro-aggregates. D3 is also associated with the development of a discontinuous axial plane S3 foliation marked by SPO and LPO of green Amp1, Wm2, Chl1, Ep3, green Bt1 and Ttn. Pmp partly replaces Lws and syn-D2 minerals.

Summarising the inferred stable assemblages during D3 are

green Amp1+Grt3+Chl1+Wm2+Ep2±Pl±Ttn±Opq in metagabbros

and green Amp1+Chl1+Wm2+Ep3±Pmp±green Bt1±Qz±Ttn±Opq in Lws-bearing glaucophanites.

Post-D3 deformation and re-equilibration is responsible for a gentle folding of S3 foliation in Lws-bearing glaucophanites, without development of any crenulation cleavage. Locally, Wm2 is replaced by a fine-grained aggregate of Chl2-, green Bt1- and Pl-bearing veins cross-cutting the pre-existing fabrics.

5. Mineral Chemistry

We detected the mineral compositions from selected microstructural sites, chosen for their potential to reveal the transformation pathways accompanying fabric evolution, and to support P-T-d-t path reconstruction. Representative mineral analyses from metagabbros, Jd- and Lws-bearing glaucophanites are shown in Tables 3, 4 and 5 respectively. Compositional variations are detailed in Tables 1, 2, 3 of the Supplementary Materials (SM), and in diagrams (Figs 8, 9, 10 and 11) showing the compositional mineral trends, also significant for thermo-barometric estimates. Mineral compositions have been determined using a Jeol, JXA-8200 electron microprobe (WDS, accelerating voltage of 15 kV, beam current of 15 nA), operating at the "Dipartimento di

Scienze della Terra - A. Desio" of Milano University. Natural silicates have been used as standards and the results were processed for matrix effects using a conventional ZAF procedure. Mineral formulae are calculated on the basis of 12 oxygens for garnets and pumpellyites, 6 for pyroxenes, 23 for amphiboles, 22 for micas, 12.5 for epidotes, 8 for lawsonites and feldspars, 28 for chlorites. Fe^{3+} was recalculated based on the charge balance. Amphiboles classification follows IMA 2012 recommendations (Hawthorne *et alii*, 2012; Oberti *et alii*, 2012) and we use Locock (2014) spreadsheet. Pyroxenes classification is after Morimoto (1988).

5.1. Metagabbros

Chemical data suggests diopside composition for magmatic (syn-M0) Cpx1 (Fig. 8a). Differently, D1a Cpx2 has a composition ranging between omphacite and diopsidic end-members, as a function of microstructural sites (Fig. 8a). Cpx2 exolutions show a diopside-augite composition (Fig. 8a). Cpx2 in coronitic site around Cpx1 generally exhibits higher Ca and Mg and lower Na contents, leading to diopside composition (Fig. 8b). Cpx2 in Ep1 and Chl1 (ex Pl) sites displays Na-rich compositions (Fig. 8b).

D1a and D2 Grt1 and Grt2 are Mg- and Mn-poor and almost all Fe^{2+} rich (Fig. 9). Highest Ca content is recorded by Grt3 filling veins developed in coronitic metagabbros (Fig. 9c).

Chemical data show a continuous compositional variation from syn-D2 Gln1 to syn-D3 green Amp1 with a general trend of Na and Al depletion (Fig. 10a-c). Gln1 shows Na depletion and Ca-enrichment toward the rim, leading to a wide range of compositions from glaucophane to katophorite-winchite terms (Fig. 10a). They are mostly sited in Cpx1 coronas or replacing ex-

Cpx1 sites. Amphiboles associated with Pmp1 have composition ranging from actinolite to winchite (Amp1 in Fig. 10a) and syn-D3 green Amp1 are mostly Ca-rich amphiboles with actinolitic composition (g-Amp1 in Fig. 10).

Sin D2 Wm1 exhibits different composition according to the microstructural site (Fig. 10d-f). Wm1 growing within Gln1, Ep1, Grt1 and Chl1 sites have phengitic composition while those occurring in pseudomorphic aggregates together with Pmp1 and Ep1 have muscovite composition.

5.2. Jd-bearing glaucophanites

Sin D1a Jd1 cores have higher Fe^{3+} content (>0.20 a.p.f.u.) compared to rim (<0.10 a.p.f.u.) (Fig. 8c-d). D1a Grt1 has lower Fe^{2+} and higher Ca and Mn contents with respect to Grt2, whereas Mg content is <0.05 a.p.f.u. (Fig. 9). Gln1 stable during D2 has a NaB content from 1.6 and 2 a.p.f.u. Gln1 cores show lower X_{Mg} content with respect to Gln1 rims, with a more Fe-glaucophane affinity (Fig. 10a).

Wm1 is stable from D1a to D2 deformation phase. Wm1 porphyroclasts have chemical zoning from paragonitic to phengitic composition (Fig. 10d,e). Paragonitic Wm1 is characterised by Na content between 1.4-1.6 a.p.f.u. and low K (Fig. 10e); phengitic Wm1 is K-rich (1.4-1.8 a.p.f.u.) and Na-poor.

5.3. Lws-bearing glaucophanites

In Lws1, stable during D1b, the amount of Ca is 0.9 a.p.f.u. and Al ranges between 1.98-2.04 a.p.f.u. Low amount of FeO is present (0.28-63 wt%), generally being higher in Lws1 included in Grt1 porphyroclasts, and MnO occurs in traces. Sin D1b Grt1 has higher Ca and Mn content than Grt2 stable during D2, and lower Mg content (Fig. 9). These differences can

reflect variations in the bulk compositions from the different samples selected to investigate syn-D1b and syn-D2 mineral assemblages.

Sin D1b Gln1 and syn-D2 Gln2 share same chemical composition: B site is completely filled by Na and Al in octahedral coordination (Al^{VI} 6.0 a.p.f.u.), leaving T site completely filled by Si atoms (Fig. 10a). X_{Mg} has little oscillation, in the range of 0.4-0.6 and Ti content is below the detection limit. Green Amp1, stable during D3, is Ca-rich with high Mg content in octahedral coordination (Mg 3.2 a.p.f.u., Fe 1.5 a.p.f.u. and Al 0.1 a.p.f.u.), corresponding to actinolite-edenite composition (Fig. 10a). Both syn-D1b/D2 Wm1 and D3 Wm2 have phengitic composition (Fig. 10d) with Na content <0.2 a.p.f.u. (Fig. 10e) and relatively high (Fe+Mg) content (0.6-1.0 a.p.f.u.).

6. Pressure and Temperature conditions of metamorphism

Micro-structural analysis indicates that the investigated rocks preserve evidence of superposed structural and metamorphic re-equilibrations (even in volumes as small as that of a thin section), and allows the definition of paragenetic sequences. It also permits the identification of favourable sites, where microstructures suggest attainment of grain-scale equilibrium, for inferring PT conditions during each re-equilibration stage. PT values derived using critical minerals such as garnet, in which the compositional zoning suggests a heterogeneous re-equilibration, have been calculated using minerals in microstructural domains indicating textural equilibria. Physical conditions of successive re-equilibration stages have been inferred by the application of well calibrated independent thermo-barometers (Table 6), calculated mineral equilibria and experimental curves. Reaction curves and stable intersections

for each lithology have been derived by thermodynamic computational software Thermocalc version 3.37 (mode 3-Schreinemakers, Holland & Powell, 1998) and reported in Figure 11 with relative error bars from mineral compositions (Table 3-5). Inferred PT fields have been associated with each deformation stage (Fig. 11) to deduce the P-T-d-t evolution (Spalla, 1993; Johnson & Vernon, 1995). Thermo-barometric estimates and errors are shown in Table 6 and the T ranges, estimated with geothermometers, are reported in Figure 11 at pressure values representing the average estimated P. PT fields for each event consider the cross-correlation between the results of different applied methods (Fig. 11), and these are supported by the coherence with successive parageneses, which are inferred by microstructural analysis.

M1a/D1a stage, recorded by metagabbros took place at pressure above 1.4 GPa defined by the stability field of Jd, Grt and Wm (Fig. 11) and confirmed by the Si^{4+} content in Wm (Table 6). The lower temperature limit is defined by experimental curve Lws+Wm=Cpx+Wm+Qz, and Grt-Phe and Grt-Cpx thermometer define a temperature range of 440-470°C. Similar pressure conditions have also been defined for M1a/D1a stage recorded by Jd-bearing glaucophanites (P>1.3 GPa), defined by the stability fields of Jd, Grt, Wm and Ep, calculated for the analysed mineral compositions of the equilibrium assemblage (Fig. 11). Calculated intersection points Grt, Wm, Jd, Chl, Qz and Grt, Jd, Gl, Ab, Chl, Qz for Jd-bearing glaucophanites give P=1.45±0.5 GPa and T=540±30°C. Coherently, the Fe-Mg exchange between Grt and Phe (Green & Hellman, 1982), applied to mineral pairs in mutual contact in Jd-bearing glaucophanites, indicates T=510±35°C, and

calibrated barometers gives P values of ca. 1.3 GPa (Table 6).

M1b/D1b stage is recorded by Lws-bearing glaucophanites and occurs under temperature below 470°C as inferred for mineral compositions of the assemblage Gln+Lws+Grt+Wm+Ep (Table 2; Fig. 11) and from three independent thermometers (Table 6). A minimum pressure of 1.1-1.2 GPa is defined by the gradual consumption of Lws and the occurrence of Pmp (Fig. 11). The Si^{4+} content in Wm (Table 6) gives a pressure of 1.5 GPa.

D2 stage is shared by all lithologies and occurs in a temperature range of ca. 380 to 550°C, as testified by the mineral association Gln+Grt+Wm+Pmp, the gradual destabilisation of Lws in the Lws-bearing glaucophanites and the occurrence of Pl in the Jd-bearing glaucophanites (Fig. 11). The Grt-Phe and Grt-Amp geothermometers plots in the inferred T-interval. A relatively high error affects the Grt-Amp estimates because of the high Na-content of Amp (Table 6) with respect to original calibration (Graham & Powell, 1984; Ravna, 2000). The upper pressure limit is constrained by the reaction curve Ab=Jd+Qz for the Jd-bearing glaucophanites and by Pmp and Gl occurrence for Lws-bearing glaucophanites and metagabbros. The lower limit is defined for the Lws-bearing glaucophanites by the stability of Grt and Pmp, confining the P interval of D2 between 0.9 and 1.4 GPa (Fig. 11), in agreement with the estimates from independent barometers calculated for metagabbros and Jd-bearing glaucophanites (Table 6). Calculated intersection points Grt, Ep, Amp, Qz and Gl, Grt, Ep, Qz and Grt, Pmp, Wm, Amp, Ep, Qz give ranges of P=1.3±0.3 GPa and T=450±50°C (Fig. 11).

D3 stage coincides with the re-equilibration of previous mineral assemblages in the stability field of Chl, green Amp, Pl and Ep. Mineral assemblage

is indicative of a pressure below 0.9 GPa and a temperature below 380°C, in agreement with the calculated curves Grt+Lws=Pmp+Chl+Qz+Ab and Pmp+Chl+Qz=Tr+Ep (Fig. 11). Coherently the Al_{IV} content in Chl (Cathelineau, 1988) and the Fe-Mg exchange between Grt and Chl (Grambling, 1990) give T of 295±15 and 320±60, respectively (Table 6).

7. Discussion

Integrated microstructural and petrologic investigations performed on metabasites from Rocca-Canavese Thrust Sheet allowed to infer different metamorphic conditions for metagabbros, Jd- and Lws-bearing glaucophanites (Fig. 12). Metagabbros and Jd-bearing glaucophanites record an early structural and metamorphic equilibration stage (D1a) at P=1.3-1.8 GPa and T=450-550°C, under eclogite facies condition. Eclogite facies conditions have never been documented before in the RCT (Pognante, 1989a; Spalla & Zulbati, 2003) although an early HP mineral assemblage, developed during D1, has been described by Cantù *et alii* (2016). Differently, Lws-bearing glaucophanites experienced the first metamorphic stage (D1b) at lower temperature (<470°C) and pressure (1.2-1.5 GPa), under Lws-blueschist-facies condition (Fig. 12). This stage represents the metamorphic peak documented by Pognante (1989a) and Spalla & Zulbati (2003). D1a is followed by a T and P decrease during D2, whereas the D1b to D2 exhumation path is characterised by a small T-increase. From D2 on, the RCT metabasites underwent a common metamorphic evolution, under a relatively depressed thermal state (<470°C) at intermediate pressure conditions up to pumpellyite-actinolite-facies conditions (Fig. 12).

Therefore, metabasites of Rocca Canavese Thrust Sheet belong to two distinct tectono-metamorphic-units (TMUs) before D2, as indicated by the contrasted P-T-d-t paths resulting from structural and petrologic integrated analyses (Fig. 12). The first one is characterised by the exhumation of metagabbros and Jd-bearing glaucophanites from eclogite- to Ep-blueschist-facies conditions. Conversely, the second TMU (Lws-bearing glaucophanites) is characterised by an exhumation from Lws-blueschist- to Ep-blueschist-facies conditions. After syn-D2 coupling, the RCT metabasites belong to a single TMU until the final exhumation. S2 foliation, frequently mylonitic, is the most pervasive fabric in the RCT and affects metapelites, metagranitoids and glaucophanites, metagabbros and serpentinites. Even the mylonitic zone marking the tectonic contact between the RCT, the EMC and the LM started forming during D2.

The metamorphic peak of metagabbro and Jd-bearing glaucophanites reflects a P/T ratio comprised between that characterising a cold and a warm subduction zone (ca. 8°C/km) while the peak of Lws-bearing glaucophanites reflects a P/T ratio compatible with a cold subduction (ca. 6°C/km, Fig. 12). The comparison of the inferred P-climax conditions recorded during D1a and D1b stages with the thermal state predicted by the 2D numerical modelling of an ocean-continent subduction system (Roda *et alii*, 2010, 2011), suggests that they are consistent with a slab dip comprised between 30 and 45°, for a convergence rate varying from 3 to 10 cm/yr. Physical conditions of syn-D2 metamorphic imprint developed under a similar thermal regime, indicating that TMUs coupling and beginning of exhumation occurred during oceanic subduction, before continental collision. In contrast,

syn-D3 inferred PT environment is sensibly higher, consistent with the thermal state of a continental collision. However, it must be emphasized that, as already evidenced by numerical models (e.g. Gerya & Stöckhert, 2005; Meda *et alii*, 2010; Roda *et alii*, 2010, 2012; Regorda *et alii*, 2017), different thermal states recorded by different TMUs do not necessarily imply a variation in the subduction zone dynamics. Indeed, rocks subducted and exhumed in the same subduction system can record different thermal states as a function of their trajectories within the hydrated mantle wedge. Taking into account the PT or P-T-d-t evolutions inferred from LM and EMC rocks in areas close to the region here investigated (Rebay, 2003; Pelletier & Müntener, 2006; Rebay & Messiga, 2007), we deduce that the coupling between the different TMUs in the south Sesia-Lanzo Zone (RCT, EMC, LM) occurred during the earlier exhumation stages, under blueschist-facies metamorphic conditions consistent with those characterising D2 indicating a cold thermal state and, as already pointed out, suggesting a still active oceanic subduction.

The RCT consists of a tectonic mixture of metagabbros, glaucophanites and metagranitoid blocks enclosed in sheared metapelites and serpentinites (Fig. 4). The blocks size range from m to km-scale and two different P-T-d-t paths characterise the evolution of metabasites up to D2, when they are coupled together with the other rocks of the mixing zone (Fig. 12). These structural and petrological characteristics agree with those described for other subduction-related tectonic mélanges (see for example the characters describe for the Franciscan mélanges, Ernst, 2016). Moreover, other tectonic mixing in the Alps (e.g. Voltri Massif, Furgg zone, Arosa zone

and Adula-Cima Lunga nappe) have been interpreted as orogenic mélanges. Therefore, we propose that RCT can represent a tectonic mélange accreted during exhumation in the Alpine subduction channel.

8. Conclusions

The integrated use of structural and petrological analysis, validated at the regional scale by detailed structural mapping, made possible the reconstruction of the tectono-metamorphic evolution of metabasites from Rocca Canavese Thrust Sheet and the distinction of different early-Alpine (Upper Cretaceous?) TMUs. In metagabbros and Jd-bearing glaucophanites the first recorded D1a metamorphic stage was characterised by P=1.3-1.8 GPa and T=450-550°C, under eclogite facies conditions, recognised for the first time in the RCT. Differently, the early inferred D1b metamorphic stage in Lws-bearing glaucophanites developed at T<470°C and P of ca. 1.2-1.5 GPa, under Lws-blueschist-facies conditions.

The two TMUs were coupled together during the early exhumation stages in the time of D2 deformation, under Ep-blueschist-facies conditions and coherently shared the successive evolution, recorded under low-P greenschist-facies conditions, compatible with a collisional thermal state. The coupling between the two TMUs of the RCT, the EMC and the LM occurred under a cold thermal regime typical for an oceanic subduction, within a subduction channel. These features indicate that the mixing of mantle- and crust-derived rocks composing the RCT can be considered an example of subduction-related mélange accreted during exhumation in the Alpine subduction channel.

9. Acknowledgments

The authors acknowledge Linea 2, Azione A - fondi giovani ricercatori "Evoluzione strutturale delle zone attive della litosfera e modellazione geodinamica" (PSR2015-1716DZANO-M). We thank Luca Corti for helping with the cross-sections. We gratefully acknowledge the Editor William Cavazza and two anonymous reviewers for their highly constructive criticism of the text.

10. References

Babist J., Handy M.R., Konrad-Schmolke M. & Hammerschmidt K. (2006) - *Precollisional, multistage exhumation of subducted continental crust: The Sesia Zone, western Alps.* Tectonics, **25** (TC6008). doi: 10.1029/2005TC001927.

Balestro G., Festa A. & Tartarotti P. (2015) - *Tectonic significance of different block-in-matrix structures in exhumed convergent plate margins: examples from oceanic and continental HP rocks in Inner Western Alps (northwest Italy).* International Geology Review, **57** (5-8), 581–605. doi:10.1080/00206814.2014.943307.

Barnes J.D., Beltrando M., Lee C.T.A., Cisneros M., Loewy S. & Chin E. (2014) - *Geochemistry of Alpine serpentinites from rifting to subduction: A view across paleogeographic domains and metamorphic grade.* Chemical Geology, **389**, 29–47. doi:10.1016/j.chemgeo.2014.09.012.

Berger A. & Bousquet R. (2008) - *Subduction-related metamorphism in the Alps: review of isotopic ages based on petrology and their geodynamic consequences.* Geological Society, London, Special Publications, **298** (1), 117–144. doi:10.1144/SP298.7.

Bousquet R. (2008) - *Metamorphic heterogeneities within a single HP unit: Overprint effect or metamorphic mix?* Lithos, **103** (1-2), 46–69. doi: 10.1016/j.lithos.2007.09.010.

Cantù M. (2011) - *Analisi strutturale multiscala del Rocca Canavese Thrust Sheets (Zona Sesia Lanzo, Austroalpino occidentale): evoluzione tettono-*

metamorfica di materiale coinvolto nella subduzione alpina. Tesi di Dottorato, Università degli Studi di Milano.

Cantù M., Spaggiari L., Zucali M., Zanoni D. & Iole Spalla M. (2016) - *Structural analysis of a subduction-related contact in southern Sesia-Lanzo Zone (Austroalpine Domain, Italian Western Alps)*. Journal of Maps, **12** (sup1), 22–35. doi:10.1080/17445647.2016.1155925.

Caron C., Homewood P. & Wildi W. (1989) - *The original Swiss flysch: a reappraisal of the type deposits in the Swiss prealps*. Earth-Science Reviews, **26** (1), 1–45. doi:10.1016/0012-8252(89)90002-0.

Cathelineau M. (1988) - *Cation Site Occupancy in Chlorites and Illites as a Function of Temperature*. Clay Minerals, **23** (4), 471–485. doi:10.1180/claymin.1988.023.4.13.

Cavargna-Sani M., Epard J.L., Bussy F. & Ulianov A. (2014) - *Basement lithostratigraphy of the Adula nappe: implications for Palaeozoic evolution and Alpine kinematics*. International Journal of Earth Sciences, **103** (1), 61–82. doi:10.1007/s00531-013-0941-1.

Cloos M. (1993) - *Lithospheric buoyancy and collisional orogenesis: Subduction of oceanic plateaus, continental margins, island arcs, spreading ridges, and seamounts*. Geological Society of America Bulletin, **105** (6), 715. doi:10.1130/0016-7606(1993)105<0715:LBACOS>2.3.CO;2.

Cloos M. & Shreve R.L. (1988) - *Subduction-Channel Model of Prism Accrectio, Melange Formation, Sediment Subduction, and Subduction Erosion*

at Convergent Plate Margins: 2. Implication and Discussion. PaGeoph., **128** (3/4), 501–545.

Compagnoni R. (1977) - *The Sesia-Lanzo zone: high-pressure low-temperature metamorphism in the Austroalpine continental margin.* Rendiconti della Società Italiana di Mineralogia e Petrologia, **33**, 335–374.

Corti L., Alberelli G., Zanoni D. & Zucali M. (2017) - *Analysis of fabric evolution and metamorphic reaction progress at Lago della Vecchia-Valle d'Irogna, Sesia-Lanzo Zone, Western Alps.* Journal of Maps, **13** (2), 521–533. doi:10.1080/17445647.2017.1331177.

Cowan D.S. (1985) - *Structural styles in Mesozoic and Cenozoic mélanges in the western Cordillera of North America.* Geological Society of America Bulletin, **96** (4), 451. doi:10.1130/0016-7606(1985)96<451:SSIMAC>2.0.CO;2.

Dal Piaz G.V., Hunziker J.C. & Martinotti G. (1972) - *La Zona Sesia – Lanzo e l'evoluzione tettonico-metamorfica delle Alpi Nordoccidentali interne.* Memorie della Societa Geologica Italiana, **11**, 433–460.

Dale J., Holland T.J.B. & Powell R. (2000) - *Hornblendegarnetplagioclase thermobarometry: a natural assemblage calibration of the thermodynamics of hornblende.* Contributions to Mineralogy and Petrology, **140** (3), 353–362. doi:10.1007/s004100000.

Dilek Y., Festa A., Ogawa Y. & Pini G.A. (2012) - *Chaos and geodynamics: Mélanges, mélange-forming processes and their significance in*

the geological record. Tectonophysics, **568-569** (Supplement C), 1–6. doi: 10.1016/j.tecto.2012.08.002.

Ellis D.J. & Green D.H. (1979) - *An experimental study of the effect of Ca upon garnet-clinopyroxene Fe-Mg exchange equilibria*. Contributions to Mineralogy and Petrology, **71** (1), 13–22. doi:10.1007/BF00371878.

Engi M., Berger A. & Roselle G.T. (2001) - *Role of the tectonic accretion channel in collisional orogeny*. Geology, **29** (12), 1143–1146. doi: 10.1130/0091-7613(2001)029<1143:ROTTAC>2.0.CO;2.

Engi M., Bousquet R. & Berger A. (2004) - *Explanatory notes to the map: metamorphic structure of the Alps age map of the metamorphic structure of the Alps - Central Alps*. Mitteilungen der Gesellschaft der Geologie- und Bergbaustudenten in Österreich, **149**, 157–173.

England P.C. & Thompson A.B. (1984) - *Pressure–Temperature–Time Paths of Regional Metamorphism I. Heat Transfer during the Evolution of Regions of Thickened Continental Crust*. Journal of Petrology, **25** (4), 894–928. doi:10.1093/petrology/25.4.894.

Ernst W.G. (2016) - *Franciscan mélanges: coherent blocks in a low-density, ductile matrix*. International Geology Review, **58** (5), 626–642. doi: 10.1080/00206814.2015.1108879.

Ernst W.G. & Liou J.G. (2008) - *High- and ultrahigh-pressure metamorphism: Past results and future prospects*. American Mineralogist, **93**, 1771–1786. doi:10.2138/am.2008.2940.

Federico L., Crispini L., Scambelluri M. & Capponi G. (2007) - *Ophiolite mélange zone records exhumation in a fossil subduction channel.* Geology, **35**, 499–502. doi:10.1130/G23190A.1.

Ferraris C. & Compagnoni R. (2003) - *Metamorphic evolution and significance of a serpentinized peridotite slice within the Eclogitic Micaschist Complex of the Sesia-Zone (Western Alps - Italy).* Swiss Bulletin of Mineralogy and Petrology, **83**, 3–13.

Festa A., Pini G.A., Dilek Y. & Codegone G. (2010) - *Mélanges and mélange-forming processes: a historical overview and new concepts.* International Geology Review, **52** (10-12), 1040–1105. doi: 10.1080/00206810903557704.

Frisch W. (1984) - *Sedimentological response to late Mesozoic subduction in the Penninic windows of the Eastern Alps.* Geologische Rundschau, **73** (1), 33–45. doi:10.1007/BF01820359.

Froitzheim N. (2001) - *Origin of the Monte Rosa nappe in the Pennine Alps-A new working hypothesis.* Geological Society of America Bulletin, **113** (5), 604. doi:10.1130/0016-7606(2001)113<0604:OOTMRN>2.0.CO;2.

Gerya T.V. & Stöckhert B. (2005) - *Two-dimensional numerical modeling of tectonic and metamorphic histories at active continental margins.* Int J Earth Sci (Geol Rundsch), **95** (2), 250–274. doi:10.1007/s00531-005-0035-9.

Gosso G. (1977) - *Metamorphic evolution and fold history in the eclogite micaschists of the upper Gressoney valley (Sesia-Lanzo zone, Western Alps).* Rendiconti della Società Italiana di Mineralogia e Petrologia, **33**, 389–407.

Gosso G., Messiga B., Rebay G. & Spalla M.I. (2010) - *The interplay between deformation and metamorphism during eclogitization of amphibolites in the Sesia-Lanzo zone of the Western Alps.* International Geology Review, **51** (12), 1193–1219. doi:10.1080/00206810903529646.

Gosso G., Rebay G., Roda M., Spalla M.I., Tarallo M., Zanoni D. & Zucali M. (2015) - *Taking advantage of petrostructural heterogeneities in subduction- collisional orogens, and effect on the scale of analysis.* Periodico di Mineralogia, **84** (3B), 779–825. doi:10.2451/2015PM0452.

Graham C.M. & Powell R. (1984) - *A garnet?hornblende geothermometer: calibration, testing, and application to the Pelona Schist, Southern California.* Journal of Metamorphic Geology, **2** (1), 13–31. doi: 10.1111/j.1525-1314.1984.tb00282.x.

Grambling J.A. (1990) - *Internally-consistent geothermometry and H2O barometry in metamorphic rocks: The example garnet-chlorite-quartz.* Contributions to Mineralogy and Petrology, **105** (6), 617–628. doi: 10.1007/BF00306528.

Green T. & Hellman P. (1982) - *Fe-Mg partitioning between coexisting garnet and phengite at high pressure, and comments on a garnet-phengite geothermometer.* Lithos, **15** (4), 253–266. doi:10.1016/0024-4937(82)90017-2.

Guarnieri L., Nakamura E., Piccardo G.B., Sakaguchi C., Shimizu N., Vannucci R. & Zanetti A. (2012) - *Petrology, Trace Element and Sr, Nd, Hf Isotope Geochemistry of the North Lanzo Peridotite Massif (Western Alps, Italy).* Journal of Petrology, **53** (11), 2259–2306. doi:10.1093/petrology/egs049.

Guillot S., Hattori K., Agard P., Schwartz S. & Vidal O. (2009) - *Exhumation Processes in Oceanic and Continental Subduction Contexts: A Review.* In: S. Lallemand & F. Funiciello (Eds.), *Subduction Zone Dynamics*, pp. 175–204. Springer-Verlag Berlin Heidelberg. doi: 10.1007/978-3-540-87974-9.

Handy M.R. & Oberhänsli R. (2004) - *Explanatory notes to the map: metamorphic structure of the Alps age map of the metamorphic structure of the Alps - tectonic interpretation and outstanding problem.* Mitt. Österr. Miner. Ges., **149**, 201–225.

Hawthorne F.C., Oberti R., Harlow G.E., Maresch W.V., Martin R.F., Schumacher J.C. & Welch M.D. (2012) - *Nomenclature of the amphibole supergroup.* American Mineralogist, **97** (11-12), 2031–2048. doi:10.2138/am.2012.4276.

Herwartz D., Nagel T.J., Münker C., Scherer E.E. & Froitzheim N. (2011) - *Tracing two orogenic cycles in one eclogite sample by Lu-Hf garnet chronometry.* Nature Geoscience, **4** (3), 178–183. doi: 10.1038/ngeo1060.

Holland T.J.B. (1980) - *The reaction albite=jadeite+quartz determined*

experimentally in the range 600-1200 C. American Mineralogist, **65**, 129–134.

Holland T.J.B. & Powell R. (1998) - *An internally consistent thermodynamic data set for phases of petrological interest.* Journal of Metamorphic Geology, **16** (3), 309–343. doi:10.1111/j.1525-1314.1998.00140.x.

Jenny H., Frischknecht G. & Kopp J. (1923) - *Geologie der Adula.* Beitrage der Geologische Karte der Schweiz, **N.F., 51**.

Johnson S.E. & Vernon R.H. (1995) - *Inferring the timing of porphyroblast growth in the absence of continuity between inclusion trails and matrix foliations: can it be reliably done?* Journal of Structural Geology, **17** (8), 1203–1206. doi:10.1016/0191-8141(95)00021-5.

Kohn M.J. & Spear F.S. (1990) - *Two new geobarometers for garnet amphibolites, with applications to Southeastern Vermont.* American Mineralogist, **75** (1), 89–96.

Lardeaux J.M., Gosso G., Kienast J.R. & Lombardo B. (1982) - *Relations entre le métamorphisme et la déformation dans la zone Sesia-Lanzo (Alpes Occidentales) et le problème de l'é clogitisation de la croûte continentale.* Bulletin de la Societé Géologique de France, **24** (4), 793–800.

Lardeaux J.M. & Spalla M.I. (1991) - *From granulites to eclogites in the Sesia zone (Italian Western Alps): a record of the opening and closure of the Piedmont ocean.* Journal of Metamorphic Geology, **9** (1), 35–59. doi:10.1111/j.1525-1314.1991.tb00503.x.

Locock A.J. (2014) - *An Excel spreadsheet to classify chemical analyses of amphiboles following the IMA 2012 recommendations.* Computers & Geosciences, **62**, 1–11. doi:10.1016/j.cageo.2013.09.011.

Malatesta C., Crispini L., Federico L., Capponi G. & Scambelluri M. (2012) - *The exhumation of high pressure ophiolites (Voltri Massif, Western Alps): Insights from structural and petrologic data on metagabbro bodies.* Tectonophysics, **568**, 102–123. doi: 10.1016/j.tecto.2011.08.024.

Manzotti P., Ballèvre M., Zucali M., Robyr M. & Engi M. (2014) - *The tectonometamorphic evolution of the Sesia-Dent Blanche nappes (internal Western Alps): review and synthesis.* Swiss Journal of Geosciences, **107** (2-3), 309–336. doi:10.1007/s00015-014-0172-x.

Massonne H.J. & Schreyer W. (1987) - *Phengite geobarometry based on the limiting assemblage with K-feldspar, phlogopite, and quartz.* Contributions to Mineralogy and Petrology, **96** (2), 212–224. doi: 10.1007/BF00375235.

Meda M., Marotta A.M. & Spalla M.I. (2010) - *The role of mantle hydration into the continental crust recycling in the wedge region.* Geological Society, London, Special Publications, **332** (1), 149–172. doi: 10.1144/SP332.10.

Milnes A.G., Greller M. & Müller R. (1981) - *Sequence and style of major post-nappe structures, Simplon-Pennine Alps.* Journal of Structural Geology, **3** (4), 411–420. doi:10.1016/0191-8141(81)90041-9.

Morimoto N. (1988) - *Nomenclature of Pyroxenes.* Mineralogy and Petrology, **39** (1), 55–76. doi:10.1007/BF01226262.

Müntener O., Piccardo G.B., Polino R. & Zanetti A. (2005) - *Revisiting the Lanzo peridotite (NW-Italy): 'Asthenospherization' of ancient mantle lithosphere.* Ofioliti, **30** (2), 111–124.

Oberhänsli R., Hunziker J.C., Martinotti G. & Stern W.B. (1985) - *Geochemistry, geochronology and petrology of Monte Mucrone: An example of EO-alpine eclogitization of Permian granitoids in the Sesia-Lanzo Zone, Western Alps, Italy.* Chemical Geology, **52** (2), 165–184. doi: 10.1016/0168-9622(85)90016-8.

Oberti R., Cannillo E. & Toscani G. (2012) - *How to name amphiboles after the IMA2012 report: rules of thumb and a new PC program for monoclinic amphiboles.* Periodico di Mineralogia, **81** (2). doi: 10.2451/2012PM0015.

Pelletier L. & Müntener O. (2006) - *High-pressure metamorphism of the Lanzo peridotite and its oceanic cover, and some consequences for the Sesia-Lanzo zone (northwestern Italian Alps).* Lithos, **90** (1-2), 111–130. doi:10.1016/j.lithos.2006.01.006.

Piccardo G.B. (2010) - *The Lanzo peridotite massif, Italian Western Alps: Jurassic rifting of the Ligurian Tethys.* Geological Society, London, Special Publications, **337** (1), 47–69.

Pognante U. (1989a) - *Lawsonite, blueschist and eclogite formation in the*

southern Sesia Zone (Western Alps, Italy). European Journal of Mineralogy, **1**, 89–104.

Pognante U. (1989b) - *Tectonic implications of lawsonite formation in the Sesia zone (Western Alps).* Tectonophysics, **162** (3-4), 219–227. doi: 10.1016/0040-1951(89)90245-X.

Pognante U., Compagnoni R. & Gosso G. (1980) - *Micro-Mesostructural relatinships in the continental eclogitic rocks of the Sesia-Lanzo Zone (Italian Western Alps): a record of subduction cycle.* Rendiconti della Società Italiana di Mineralogia e Petrologia, **36** (1), 169–186.

Pognante U., Rösli U. & Toscani L. (1985) - *Petrology of ultramafic and mafic rocks from the Lanzo peridotite body (Western Alps).* Lithos, **18**, 201–214. doi:10.1016/0024-4937(85)90025-8.

Polino R., Dal Piaz G.V. & Gosso G. (1990) - *Tectonic erosion at the Adria margin and accretionary processes for the Cretaceous orogeny of the Alps.* Mémoires de la Societé Géologique de France, **156**, 345–367.

Rampone E., Borghini G., Romairone A., Abouchami W., Class C. & Goldstein S.L. (2014) - *Sm-Nd geochronology of the Erro-Tobbio gabbros (Ligurian Alps, Italy): Insights into the evolution of the Alpine Tethys.* Lithos, **205**, 236–246. doi:10.1016/j.lithos.2014.07.012.

Ravna E.K. (2000) - *Distribution of Fe2+ and Mg between coexisting garnet and hornblende in synthetic and natural systems: an empirical calibration of the garnethornblende FeMg geothermometer.* Lithos, **53** (3-4), 265–277. doi:10.1016/S0024-4937(00)00029-3.

Raymond L.A. (1984) - *Classification of mélanges.* In: L.A. Raymond (Ed.), *Mélanges: Their Nature, Origin, and Significance.* Geological Society of America. doi:10.1130/SPE198-p7.

Rebay G. (2003) - *A metamorphic map of the Corio and Monastero gabbro (Southern Sesia-Lanzo zone, NW Italy).* Memorie Scienze Geologiche, **55**, 21–30.

Rebay G. & Messiga B. (2007) - *Prograde metamorphic evolution and development of chloritoid-bearing eclogitic assemblages in subcontinental metagabbro (Sesia-Lanzo zone, Italy).* Lithos, **98** (1-4), 275–291. doi: 10.1016/j.lithos.2007.04.002.

Rebay G. & Spalla M.I. (2001) - *Emplacement at granulite facies conditions of the Sesia-Lanzo metagabbros: an early record of Permian rifting?* Lithos, **58** (3-4), 85–104. doi:10.1016/S0024-4937(01)00046-9.

Regorda A., Roda M., Marotta A.M. & Spalla M.I. (2017) - *2-D numerical study of hydrated wedge dynamics from subduction to post-collisional phases.* Geophysical Journal International, **211** (2), 952–978. doi:10.1093/gji/ggx336.

Ring U., Ratschbacher L. & Frisch W. (1988) - *Plate-boundary kinematics in the Alps: Motion in the Arosa suture zone.* Geology, **16** (8), 696. doi:10.1130/0091-7613(1988)016<0696:PBKITA>2.3.CO;2.

Ring U., Ratschbacher L., Frisch W., Dürr S. & Borchert S. (1990) - *The internal structure of the Arosa Zone (Swiss-Austrian Alps).* Geologische Rundschau, **79** (3), 725–739. doi:10.1007/BF01879211.

Roda M., Marotta A.M. & Spalla M.I. (2010) - *Numerical simulations of an ocean-continent convergent system: Influence of subduction geometry and mantle wedge hydration on crustal recycling.* Geochemistry, Geophysics, Geosystems, **11** (5), 1–21. doi:10.1029/2009GC003015.

Roda M., Marotta A.M. & Spalla M.I. (2011) - *The effects of the overriding plate thermal state on the slab dip in an ocean-continent subduction system.* Compte Rendu Academie des Sciences Paris, **343**, 323–330. doi: 10.1016/j.crte.2011.01.005.

Roda M., Spalla M.I. & Marotta A.M. (2012) - *Integration of natural data within a numerical model of ablative subduction: a possible interpretation for the Alpine dynamics of the Austroalpine crust.* Journal of Metamorphic Geology, **30** (9), 973–996. doi:10.1111/jmg.12000.

Salvi F., Spalla M.I., Zucali M. & Gosso G. (2010) - *Three-dimensional evaluation of fabric evolution and metamorphic reaction progress in polycyclic and polymetamorphic terrains: a case from the Central Italian Alps.* Geological Society, London, Special Publications, **332**, 173–187. doi:10.1144/SP332.11.

Sandmann S., Nagel T.J., Herwartz D., Fonseca R.O.C., Kurzawski R.M., Münker C. & Froitzheim N. (2014) - *Lu-Hf garnet systematics of a polymetamorphic basement unit: new evidence for coherent exhumation of the Adula Nappe (Central Alps) from eclogite-facies conditions.* Contributions to Mineralogy and Petrology, **168** (5), 1075. doi: 10.1007/s00410-014-1075-6.

Scambelluri M., Pennacchioni G., Gilio M., Bestmann M., Plümper O. & Nestola F. (2017) - *Fossil intermediate-depth earthquakes in subducting slabs linked to differential stress release.* Nature Geoscience, **10** (12), 960–966. doi:10.1038/s41561-017-0010-7.

Schuster R. & Stüwe K. (2008) - *Permian metamorphic event in the Alps.* Geology, **36**, 603–606. doi:10.1130/G24703A.1.

Schwartz S. (2000) - *The diversity of eclogitic metamorphism in the Monviso ophiolitic complex, western Alps, Italy.* Geodinamica Acta, **13** (2), 169–188. doi:10.1016/S0985-3111(00)00112-1.

Spalla M.I. (1993) - *Microstructural control on the P-T path construction in metapelites of the Austroalpine crust (Texel Gruppe, Eastern Alps).* Schweizerische Mineralogische Und Petrographische Mitteilungen, **81** (197-212).

Spalla M.I., De Maria L., Gosso G., Miletto M. & Pognante U. (1983) - *Deformazione e metamorfismo della Zona Sesia Lanzo meridionale al contatto con la falda piemontese e con il massiccio di Lanzo, Alpi occidentali.* Memorie della Societa Geologica Italiana, **26**, 499–514.

Spalla M.I., Gosso G., Marotta A.M., Zucali M. & Salvi F. (2010) - *Analysis of natural tectonic systems coupled with numerical modelling of the polycyclic continental lithosphere of the Alps.* International Geology Review, **52** (10-12), 1268–1302. doi:10.1080/00206814.2010.482737.

Spalla M.I., Lardeaux J.M., Dal Piaz G.V. & Gosso G. (1991) -

Métamorphisme et tectonique à la marge externe de la zone Sesia-Lanzo (Alpes occidentales). Memorie di Scienze Geologiche, **43**, 361–369.

Spalla M.I., Lardeaux J.M., Piaz G.v.D., Gosso G. & Messiga B. (1996) - *Tectonic significance of Alpine eclogites.* Journal of Geodynamics, **21** (3), 257–285. doi:10.1016/0264-3707(95)00033-X.

Spalla M.I., Zanoni D., Marotta A.M., Rebay G., Roda M., Zucali M. & Gosso G. (2014) - *The transition from Variscan collision to continental break-up in the Alps: insights from the comparison between natural data and numerical model predictions.* Geological Society, London, Special Publications, **405** (1), 363–400. doi:10.1144/SP405.11.

Spalla M.I. & Zulbati F. (2003) - *Structural and petrographic map of the southern Sesia-Lanzo Zone (Monte Soglio - Rocca Canavese, Western Alps, Italy).* Memorie di Scienze Geologiche, Padova, **55**, 119–127.

Stöckhert B. & Gerya T.V. (2005) - *Pre-collisional high pressure metamorphism and nappe tectonics at active continental margins: a numerical simulation.* Terra Nova, **17**, 102–110. doi:10.1111/j.1365-3121.2004.00589.x.

Stünitz H. (1989) - *Partitioning of metamorphism and deformation in the boundary region of the Seconda Zona Diorito-Kinzigitica.* Tesi di Dottorato, Geologisches Institut der Eidg. Technischen Hochschule und der Universität, Zürich.

Tartarotti P., Festa A., Benciolini L. & Balestro G. (2017) - *Record of Jurassic mass transport processes through the orogenic cycle:*

Understanding chaotic rock units in the high-pressure Zermatt-Saas ophiolite (Western Alps). Lithosphere, **9** (3), 399. doi:10.1130/L605.1.

Trommsdorff V. (1990) - *Metamorphism and tectonics in the Central Alps: The Alpine lithospheric mélange of Cima Lunga and Adula.* Memorie della Società Geologica Italiana, **45**, 39–49.

Vuichard J.P. (1987) - *Conditions PT du métamorphisme ante alpin dans la seconde zone diorito-kinzigitique (Zone Sesia-Lanzo, Alpes occidentales).* Schweizerische Mineralogische Und Petrographische Mitteilungen, **67**, 257–271.

Wakabayashi J. (2015) - *Anatomy of a subduction complex: architecture of the Franciscan Complex, California, at multiple length and time scales.* International Geology Review, **57** (5-8), 669–746. doi: 10.1080/00206814.2014.998728.

Wheeler J. & Butler R.W. (1993) - *Evidence for extension in the western Alpine orogen: the contact between the oceanic Piemonte and overlying continental Sesia units.* Earth and Planetary Science Letters, **117** (3-4), 457–474. doi:10.1016/0012-821X(93)90097-S.

Whitney D.L. & Evans B.W. (2010) - *Abbreviations for names of rock-forming minerals.* American Mineralogist, **95**, 185–187. doi: 10.2138/am.2010.3371.

Williams P.F. & Compagnoni R. (1983) - *Deformation and metamorphism in the Bard area of the Sesia Lanzo Zone, Western Alps, during*

subduction and uplift. Journal of Metamorphic Geology, **1** (2), 117–140. doi:10.1111/j.1525-1314.1983.tb00268.x.

Winkler W. (1988) - *Mid- to early Late Cretaceous flysch and melange formations in the western part of the Eastern Alps*. Jahrb Geol Bundesanst, **131**, 341–389.

Zanoni D., Bado L., Spalla M.I., Zucali M. & Gosso G. (2008) - *Structural analysis of the Northeastern margin of the tertiary intrusive stock of Biella (Western Alps, Italy)*. Boll. Soc. Geol. It. (Ital. J. Geosci.), **127** (1), 125–140.

Zanoni D., Spalla M.I. & Gosso G. (2010) - *Structure and PT estimates across late-collisional plutons: constraints on the exhumation of western Alpine continental HP units*. International Geology Review, **52** (10), 1244–1267. doi:10.1080/00206814.2010.482357.

Zucali M. (2011) - *Coronitic microstructures in patchy eclogitised continental crust: the Lago della Vecchia Permian metagranite (Sesia-Lanzo Zone, Western Italian Alps)*. Journal of The Virtual Explorer, **38** (7).

Zucali M., Spalla I. & Gosso G. (2002) - *Strain partitioning and fabric evolution as a correlation tool: the example of the Eclogitic Micaschists Complex in the Sesia-Lanzo Zone (Monte Mucrone-Monte Mars, Western Alps, Italy)*. Schweiz. Mineral. Petrogr. Mitt., **82**, 429–454.

Zucali M. & Spalla M.I. (2011) - *Prograde lawsonite during the flow of continental crust in the Alpine subduction: Strain vs. metamorphism partitioning, a field-analysis approach to infer 5 tectonometamorphic evolutions*

(Sesia-Lanzo Zone, Western Italian Alps). Journal of Structural Geology, **33**, 381–398. doi:10.1016/j.jsg.2010.12.006.

Zucali M., Spalla M.I., Gosso G., Racchetti S. & Zulbati F. (2004) - *Prograde LWS-KY Transition During Subduction Of The Alpine Continental Crust Of The Sesia- Lanzo Zone: The Ivozio Complex*. Journal of the Virtual Explorer, Electronic Edition, **16** (4), 1–21.

Figure 1: Tectonic sketch map of the Sesia-Lanzo Zone (SLZ). Rocca Canavese Thrust Sheet (RCT) is located in the South SLZ, between Eclogitic Micaschists Complex (EMC) and Canavese Zone (CZ).

Figure 2: Lithological map of Rocca Canavese Thrust Sheet (RCT) redrawn after Cantù *et alii* (2016). The mylonitic zone marks the contact between the RCT and Eclogitic Micaschists Complex (EMC) or Lanzo Massif (LM). The RCT consists of a mixing between mantle- and crust-derived lithologies.

Figure 3: Geological cross-sections. Legend and location of sections are reported in Fig. 2.

Figure 4: Metabasites of the RCT and different meso-structures. a) Small-scale block of metagranite within serpentinite matrix. b) Metre-scale block of metagabbro within serpentinite matrix. c) S2 mylonitic foliation in Lws-bearing glaucophanites. d) D3 folding of S2 foliation in Lws-bearing glaucophanites. e) S2 mylonitic foliation in Jd-bearing glaucophanites. f) D3 folding of S2 foliation in Jd-bearing glaucophanites and development of a discontinuous S3 foliation. g) Coronitic relict domains in metagabbros, wrapped by S2. h) Relict magmatic layering in poorly deformed metagabbros.

Figure 5: Microstructures in metagabbros. a) Cpx2 occurring as Cpx1 coronas; long side of photomicrograph (LSP) 0.86 mm. b) Cpx1 rimmed by Cpx2 and ex-Pl site replaced by Grt1 and Cpx2; LSP 0.86 mm. c) Interstitial ex-Pl sites between Cpx1 porphyroclasts replaced by Pmp1+Chl1 and Wm1+Chl1; LSP 0.86 mm. d) Crossed polar image of Fig. 5c; LSP 0.86 mm. e) Relicts of Cpx2 (see 4f) within Pmp1 and Chl1 sites; LSP 0.86 mm. f) Back-Scattered Electron (BSE) image of squared area located on Fig. 5e.

Figure 6: Microstructures in Jd-bearing glaucophanites. a) S1 foliation marked by elongated Jd-rich domains alternating with Gln1 and Grt2-rich layers; LSP 3.30 mm. b) Crossed polar image of Fig. 6a; LSP 3.30 mm. c) BSE image of squared area in Fig. 6c. d) Jd1 partially replaced by Gln1; LSP 0.86 mm. e) Crossed polar image of Fig. 6d to highlight blue interference colour for Jd-cores; LSP 0.86 mm. f) BSE image of squared area of Fig. 6d.

Figure 7: Microstructures in Lws-bearing glaucophanites. a) S2 films marked by Gln2+Wm1 and lithons hosting S1 foliation marked by Gnl1, Wm1 and Lws1; LSP 3.30 mm. b) Crossed polar image of Fig. 7a; LSP 3.30 mm. c) BSE image showing S2 foliation underlined by Wm1 and Pmp1 and S1 relict fabric marked by Gln1. d) S1 foliation marked by Lws1 and Wm1 SPO; LSP 3.30 mm. e) S1 foliation marked by Lws1 and Wm1 SPO; LSP 0.86 mm. f) Crossed polar image of Fig. 7e; LSP 0.86 mm.

Figure 8: Compositional variations of Px in metagabbros and Jd-bearing glaucophanites. Cpx1 has diopside composition, whereas Cpx2 shows different composition as a function of the microstructural site: Cpx2 coronas on Cpx1 is diopside while Cpx2 replacing ex-Pl sites is omphacite. Jd1 has composition variable from core to rim. Legend: red squares = Cpx1 porphyroclasts in metagabbros (Mg); orange squares = Cpx2 exolutions in Cpx1 porphyroclasts in metagabbros; blue squares = Cpx2 in metagabbros; blue circles = Jd1 in Jd-bearing glaucophanites (Jd-Gl).

Figure 9: Compositional variation of Grt in all rocks. See text for details in compositional variations. Scale along axes in panels a and b may be different from 0-100%.

Figure 10: Compositional variation of Amp (a, b and c) and Wm (d, e and f) in the RCT metabasites. Amphiboles range between glaucophane to actinolite. White micas range from phengite to muscovite. Some high paragonite content is detected for micas from Jd-bearing glaucophanites.

Figure 11: PT conditions for the three lithologies inferred from the integration of thermobarometers, comparison of natural assemblages with experimental univariant equilibria, calculated reaction curves and stable intersections.

Figure 12: P-T-d history inferred from PT-estimates. In the insets the representation of dominant fabric and mineral assemblage for each stage is shown. Metamorphic facies after (Ernst & Liou, 2008): GS=greenschist; Ep-A=epidote-bearing amphibolite; BS=blueschists; AM=amphibolite; EC=eclogite; HGR=high pressure granulite; GR=granulite. Geotherms: Vi=stable geotherms (England & Thompson, 1984) for continental crust; 3a) warm subduction zones, 3b) cold subduction zones (Cloos, 1993).

Table 1: Mineral associations and dominant fabrics in the deformed rocks of the RCT and Mylonitic zone.

lithologies	Description	Stage and Fabric			
		D1	D2	D3	D4
Metapelites	Alternate layers of Qz+Pl+Ep and Amp+Wm+Chl. Locally Qz-rich layers alternate with Jd+Wm bearing layers	S1 foliation marked by SPO of Gln, Wm, Qz and rare Grt, Ep and Op. Locally S1 mylonitic foliation marked by alternating Jd+Wm±Ep±Grt and Qz-rich layers, wrapping Grt, Jd and Ep porphyroblasts.	S2 defined by Qz+Wm and Gln+Qz compositional layering.	Isoclinal folding associated with S3 axial plane foliation marked by SPO of Act+Chl+Wm	Mm- to cm- scale crenulation of S3 foliation locally associated with rough foliation marked by fine-grained Chl and Wm
Orthogneiss	Layers of fine-grained Amp+Wm alternating with Qz-Kfs rich layers at mm- to cm-scale		S2 mylonitic foliation marked by mm- thick Gln+Wm+Ep and Kfs+Qz compositional layering	S3 mylonitic foliation marked by SPO and LPO of Act+Wm±Qz	
Serpentinite	Widely serpentinised granoblastic peridotite with relics of Cpx and Sp locally preserved in foliated types with mylonitic texture		Generally mylonitic S2 foliation marked by SPO of Srp and Op trails	D3 crenulation with a 10 cm wavelength, locally associated with a differentiated S3 crenulation cleavage marked by SPO of Srp.	
Glaucophanite	Mm- to cm-thick alternating layers of Gln+Wm and Qz+Ep	Omp, Grt and Lws relicts	S2 marked by mm-thick Gln+Wm and Ep+Qz compositional layering	S3 foliation marked by compositional layering of Act+Chl+Wm and Ep±Pmp+Qz layers.	
Metagabbro	Generally with coronitic or tectonitic fabric. In granoblastic texture Cpx porphyroclasts are preserved. Cpx is partially replaced by Gln and Cpx2. Pl replaced by Ep+Wm.	Omp, Grt and Lws relicts	Discontinuous S2 foliation marked by SPO of Gln+Wm+Ep and Grt trails±Pmp		

Table 2: Summary of deformation stages with characteristic structures and mineral associations.

Event	Stage	Structures	Mineral Association
		Metagabbros	
0	M0	coronitic	Cpx1, Opx1, Pl
1	M1a	coronitic	Cpx2±Grt1
2	M2, D2	S2 mylonitic foliation	Gln1+Grt2+Wm1+Ep1±Pmp1±Chl1
3	M3, D3	PA3 folding, S3 discontinuous foliation	green Amp1+Grt3+Chl2+Wm2+Ep2±Pmp2±Pl±Ttn±Opq
		Jd-bearing glaucophanites	
1	M1a, D1a	coronitic, S1 mylonitic foliation	Jd1+Wm1+Grt1+Ep1±Ttn±Qz
2	M2, D2	S2 continuous foliation	Gln1+Grt2+Ep2±Chl1±Pl±Wm1±Qz±Opq
		Lws-bearing glaucophanites	
1	M1b, D1b	coronitic, S1 mylonitic foliation	Gln1+Wm1+Grt1+Lws1+Ep1±Ttn±Qz
2	M2, D2	S2 mylonitic foliation	Gln2+Grt2+Wm1+Qz±Ep2±Pmp1±Ttn±Opq
3	M3, D3	PA3 folding, S3 discontinuous foliation	green Amp1+Chl1+Wm2+Ep3±Pmp2±green Bt1±Qz±Ttn±Opq

Table 3: Representative analysis of main minerals of metagabbros. [a]: corona on Cpx1; [b]: exolution in Cpx1; [c]: included in Pmp1.

Mineral	Grt1	Grt2	Cpx1	Cpx2[a]	Cpx2[b]	Cpx2[c]	Gln	Amp1	Ep1	Wm1
SiO2	37.31	38.58	49.10	55.79	50.40	56.14	55.40	55.75	39.26	50.55
TiO2	0.00	0.15	0.96	0.09	0.66	0.21	0.04	0.07	0.02	0.00
Al2O3	21.92	21.90	6.78	11.81	6.07	9.62	12.69	1.36	31.90	26.76
Cr2O3	0.00	0.06	0.07	0.04	0.06	0.10	0.08	0.03	0.00	0.00
FeO	30.73	13.38	7.81	7.52	7.40	8.39	15.43	12.81	3.37	3.09
MnO	1.31	4.56	0.24	0.10	0.20	0.14	0.02	0.12	0.08	0.00
MgO	0.36	0.17	10.95	5.93	12.10	8.28	6.35	15.69	0.06	3.34
CaO	9.40	21.23	20.11	11.70	22.25	10.22	1.08	11.33	23.77	1.12
Na2O	0.02	0.00	2.41	7.39	0.75	7.37	6.87	0.91	0.02	0.18
K2O	0.00	0.00	0.21	0.00	0.01	0.02	0.05	0.05	0.00	9.65
Sum	101.05	100.03	98.64	100.38	99.92	100.49	98.01	98.12	98.49	94.69
Ox	12.00	12.00	6.00	6.00	6.00	6.00	23.00	23.00	12.50	22.00
Si	2.97	3.00	1.83	1.99	1.87	2.00	7.79	7.95	2.98	6.80
Ti	0.00	0.01	0.03	0.00	0.02	0.01	0.00	0.01	0.00	0.00
Al	2.05	2.01	0.30	0.50	0.27	0.40	2.10	0.23	2.86	4.24
Cr	0.00	0.00	0.00	0.00	0.00	0.00	0.01	0.00	0.00	0.00
Fe2+	2.04	0.87	0.07	0.20	0.22	0.15	1.81	1.53	0.05	0.35
Fe3+	0.00	0.00	0.18	0.02	0.01	0.10	0.00	0.00	0.16	0.00
Mn	0.09	0.30	0.01	0.00	0.01	0.00	0.00	0.01	0.01	0.00
Mg	0.04	0.02	0.61	0.32	0.67	0.44	1.33	3.34	0.01	0.67
Ca	0.80	1.77	0.80	0.45	0.88	0.39	0.16	1.73	1.93	0.16
Na	0.00	0.00	0.17	0.51	0.05	0.51	1.87	0.25	0.00	0.05
K	0.00	0.00	0.01	0.00	0.00	0.00	0.01	0.01	0.00	1.66
Sum	8.00	7.98	4.30	4.50	4.27	4.40	15.09	15.06	8.00	13.93

Table 4: Representative analysis of main minerals of Jd-bearing glaucophanites.

Mineral	Jd1	Grt1	Grt2	Gln1	Wm1	Chl1
SiO2	59.34	37.27	37.13	55.89	51.88	26.05
TiO2	0.00	0.06	0.08	0.03	0.06	0.02
Al2O3	24.31	19.94	20.71	11.48	26.70	20.69
Cr2O3	0.00	0.00	0.01	0.01	0.00	0.10
FeO	1.57	22.03	37.33	20.02	2.02	27.38
MnO	0.03	8.94	1.19	0.00	0.02	0.25
MgO	0.05	0.30	0.28	3.58	3.41	14.46
CaO	0.37	9.43	5.12	0.21	0.06	0.01
Na2O	15.16	0.04	0.04	7.53	0.25	0.00
K2O	0.00	0.01	0.01	0.00	10.00	0.01
Sum	100.83	98.03	101.90	98.75	94.39	88.98
Ox	6.00	12.00	12.00	23.00	22.00	28.00
Si	1.99	3.05	2.98	7.95	6.94	5.46
Ti	0.00	0.00	0.00	0.00	0.01	0.00
Al	0.96	1.93	1.96	1.92	4.21	5.11
Cr	0.00	0.00	0.00	0.00	0.00	0.02
Fe2+	0.00	1.51	2.50	2.38	0.23	4.80
Fe3+	0.04	0.00	0.00	0.00	0.00	0.00
Mn	0.00	0.62	0.08	0.00	0.00	0.05
Mg	0.00	0.04	0.03	0.76	0.68	4.52
Ca	0.01	0.83	0.44	0.03	0.01	0.00
Na	0.99	0.01	0.01	2.08	0.06	0.00
K	0.00	0.00	0.00	0.00	1.71	0.00
Sum	4.00	7.98	8.03	15.12	13.84	19.97

Table 5: Representative analysis of main minerals of Lws-bearing glaucophanites.

Mineral	Gln1	Gln2	Amp1	Grt1	Grt2	Lws	Wm1	Wm2	Ttn
SiO2	58.16	56.20	52.39	37.21	38.05	38.12	53.00	51.74	35.03
TiO2	0.03	0.05	0.00	0.11	0.00	0.04	0.07	0.13	32.47
Al2O3	11.87	11.41	1.28	21.84	21.37	31.46	23.03	29.15	3.66
Cr2O3	0.06	0.06	0.00	0.00	0.10	0.01	0.05	0.01	0.33
FeO	12.79	10.12	12.30	18.57	29.14	0.39	2.41	1.96	0.21
MnO	0.00	0.02	0.33	8.92	0.69	0.03	0.11	0.00	0.05
MgO	7.43	8.82	14.52	0.57	9.66	0.01	4.46	3.01	0.02
CaO	0.18	0.51	11.90	13.42	0.98	16.08	0.03	0.00	27.36
Na2O	7.66	7.57	0.73	0.00	0.00	0.01	0.07	0.31	0.04
K2O	0.00	0.03	0.04	0.00	0.01	0.01	9.88	10.34	0.12
Sum	98.18	94.80	93.49	100.64	100.01	86.19	93.11	96.65	99.29
Ox	23.00	23.00	23.00	12.00	12.00	8.00	22.00	22.00	5.00
Si	8.02	7.97	7.89	2.94	2.93	2.04	7.20	6.77	4.00
Ti	0.00	0.01	0.00	0.01	0.00	0.00	0.01	0.01	2.79
Al	1.93	1.91	0.23	2.03	1.94	1.98	3.69	4.49	0.49
Cr	0.01	0.01	0.00	0.00	0.01	0.00	0.00	0.00	0.03
Fe2+	1.47	1.20	1.55	1.23	1.88	0.02	0.27	0.21	0.02
Fe3+	0.00	0.00	0.00	0.00	0.00	0.00	0.00	0.00	0.00
Mn	0.00	0.00	0.04	0.60	0.05	0.00	0.01	0.00	0.01
Mg	1.53	1.86	3.26	0.07	1.11	0.00	0.90	0.59	0.00
Ca	0.03	0.08	1.92	1.13	0.08	0.92	0.00	0.00	3.35
Na	2.05	2.08	0.21	0.00	0.00	0.00	0.02	0.08	0.01
K	0.00	0.01	0.01	0.00	0.00	0.00	1.71	1.72	0.02
Sum	15.03	15.11	15.11	8.03	8.06	4.97	13.82	13.88	10.71

Table 6: Thermobarometric estimates for the rocks. References: [1] Al_{IV} in Chl (Catthelineau, 1988); [2] Grt-Amp (Ravna, 2000); [3] Grt-Amp (Graham & Powell, 1984); [4] Grt-Phe (Green & Hellman, 1982); [5] Grt-cPx (Ellis & Green, 1979); [6] Grt-Chl (Grambling, 1990); [7] Grt-Amp (Kohn & Spear, 1990); [8] X_{Jd} in Cpx (Holland, 1980); [9] Grt-Amp-Pl (Dale *et alii*, 2000); [10] Si^{4+} in Wm (Massonne & Schreyer, 1987).

lithologies	Stage	Temperature (°C)						Pressure (GPa)			
	Method	[1]	[2]	[3]	[4]	[5]	[6]	[7]	[8]	[9]	[10]
Metagabbros	D1a				450±10	460±10			1.2±0.03		1.4±0.05
	D2			495±60	410±40			1.1±0.2		1.4±0.3	
	D3	295±15					320±60				
Jd-glaucoph.	D1a				510±35				1.3±0.03		1.2±0.05
	D2			410±65				1.0±0.2		1.2±0.1	
	D3										
Lws-glaucoph.	D1b		440±35	420±20	415±10			0.9±0.04			1.35±0.15
	D2			470±30							
	D3										

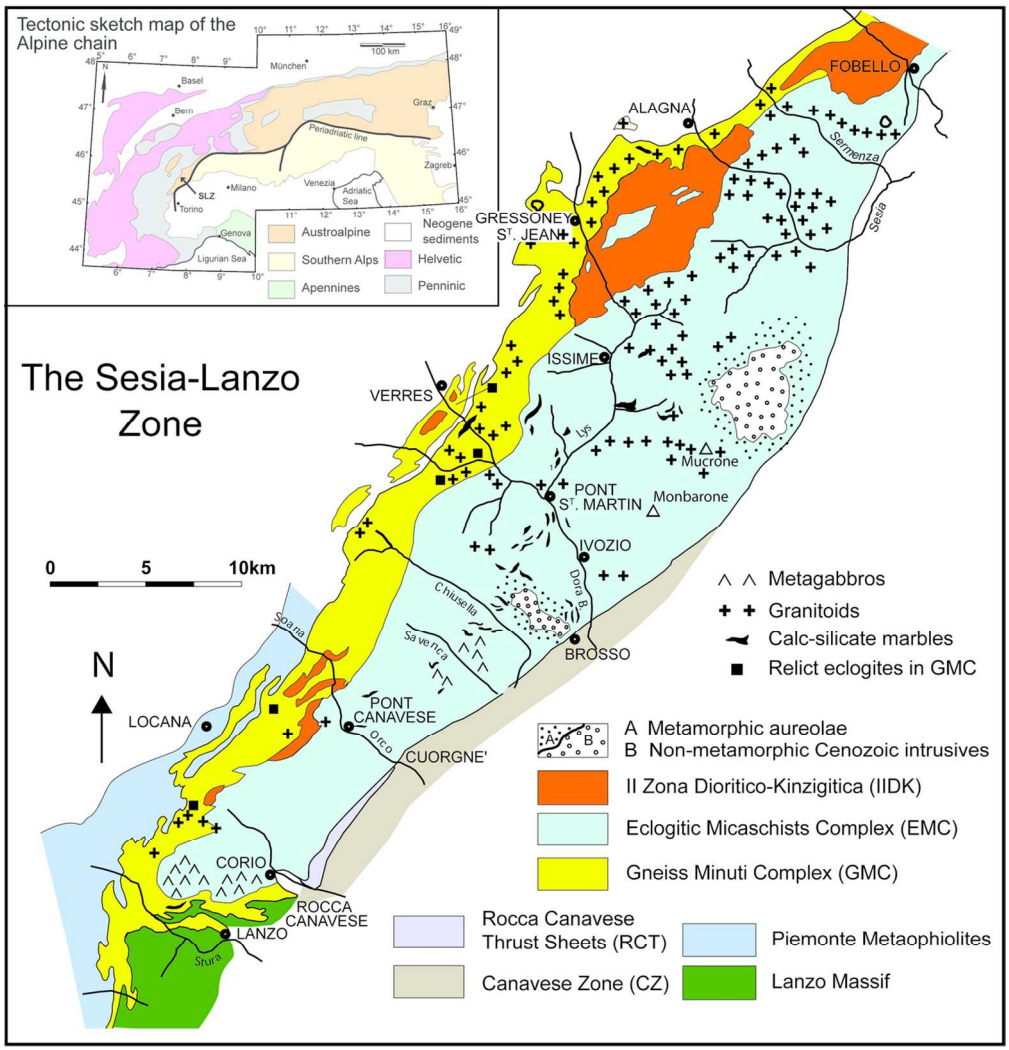

Figure 1: Tectonic sketch map of the Sesia-Lanzo Zone (SLZ). Rocca Canavese Thrust Sheet (RCT) is located in the south SLZ, between Eclogitic Micaschists Complex (EMC) and Canavese Zone (CZ).

119x123mm (300 x 300 DPI)

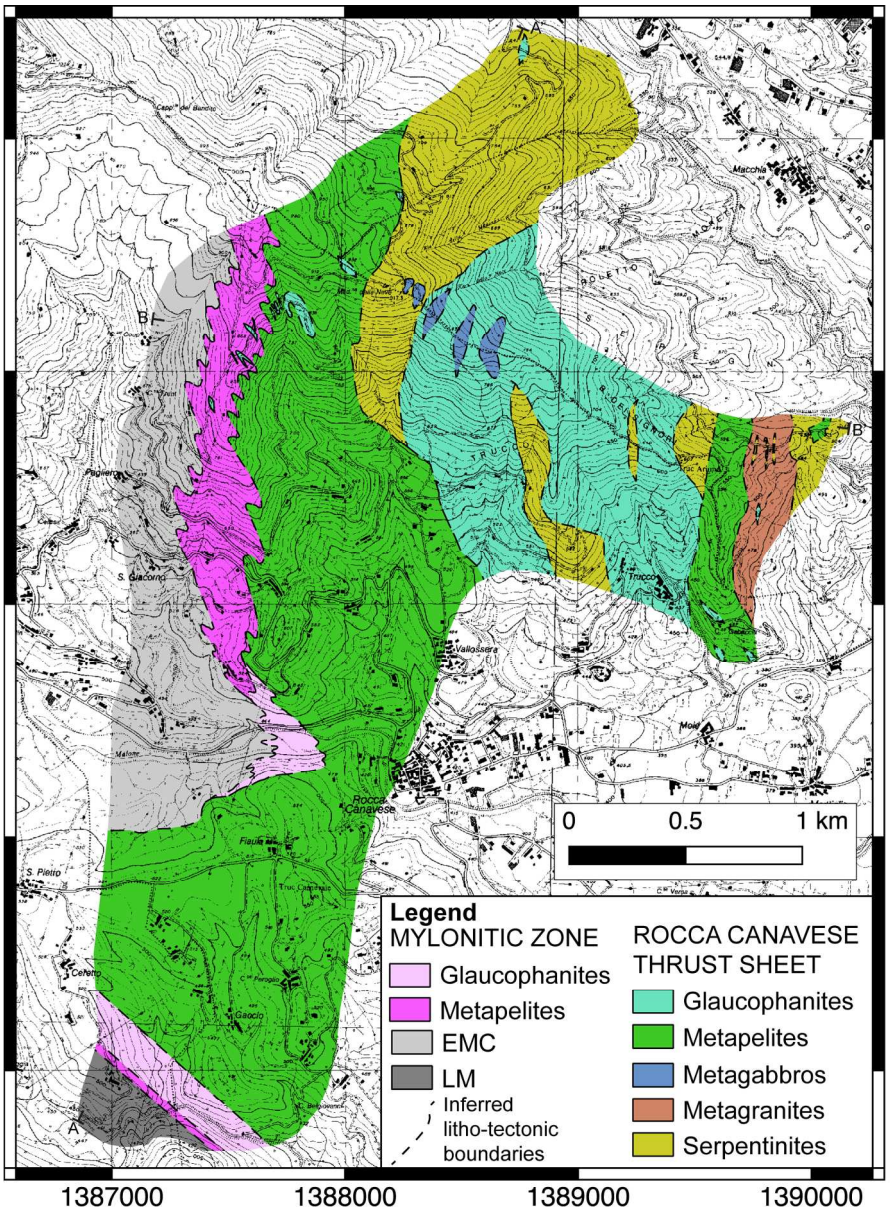

Figure2: Lithological map of Rocca Canavese Thrust Sheet (RCT) redrawn after Cantù et alii (2016). The mylonitic zone marks the contact between the RCT and Eclogitic Micaschists Complex (EMC) or Lanzo Massif (LM). The RCT consists of a mixing between mantle- and crust-derived lithologies.

156x206mm (300 x 300 DPI)

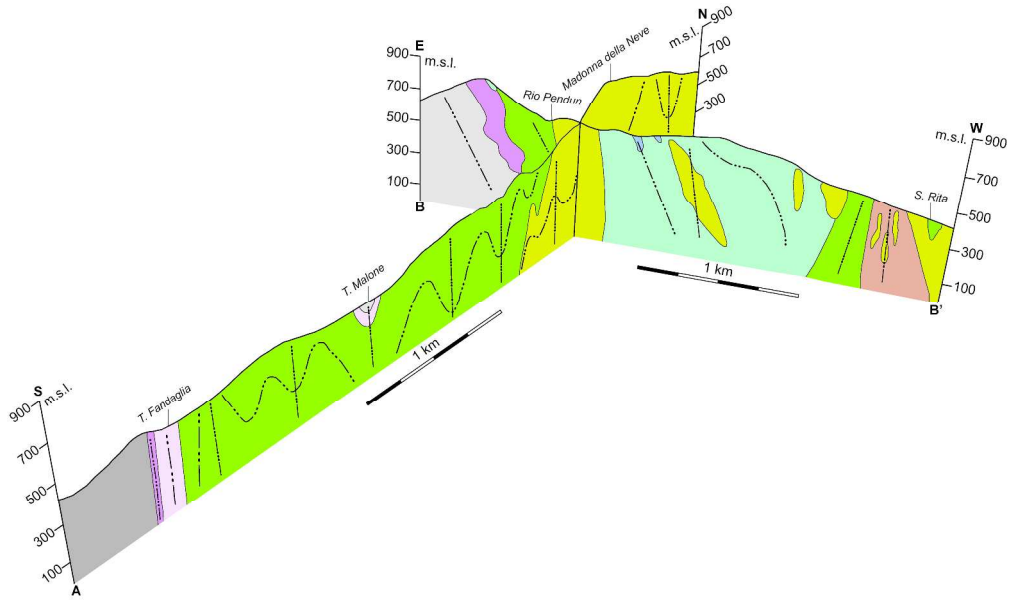

Figure 3: Geological cross-sections. Legend and location of sections are reported in Fig. 2.

313x187mm (300 x 300 DPI)

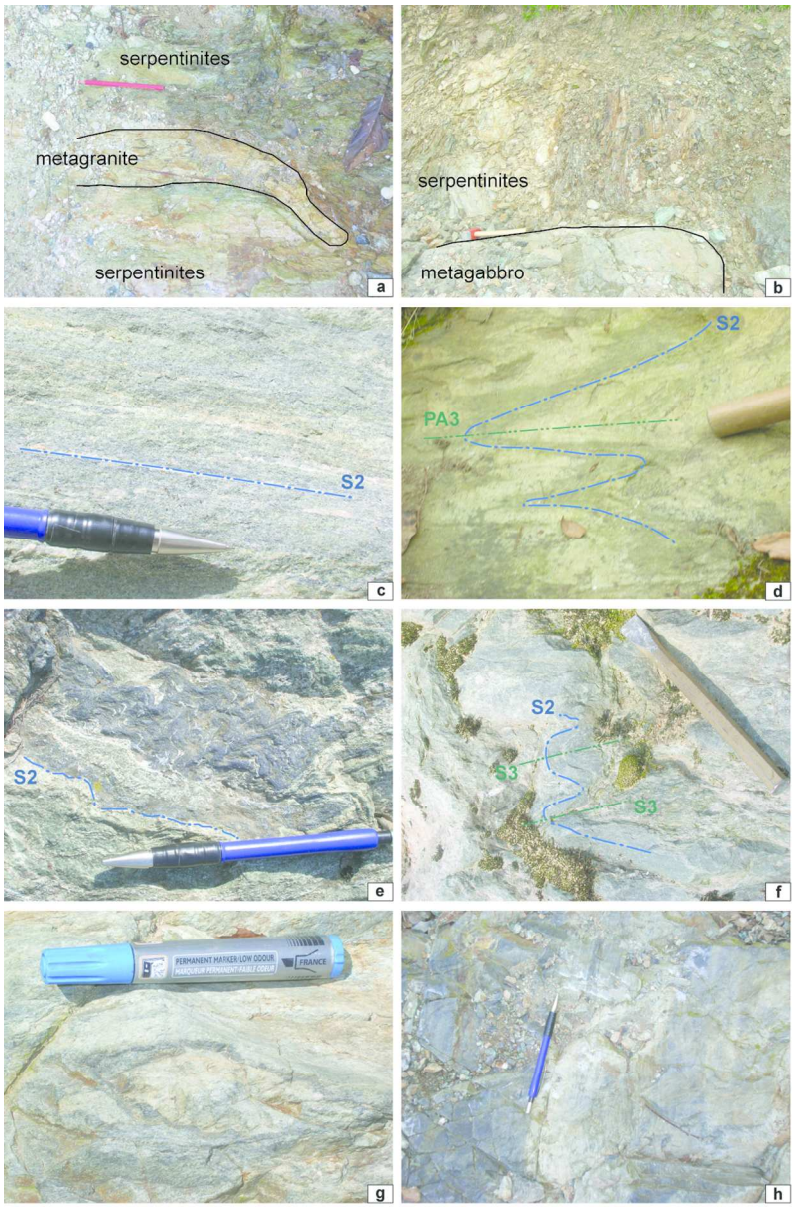

Figure 4: Metabasites of the RCT and different meso-structures. a) Small-scale block of metagranite within serpentinite matrix. b) Metre-scale block of metagabbro within serpentinite matrix. c) S2 mylonitic foliation in Lws-bearing glaucophanites. d) D3 folding of S2 foliation in Lws-bearing glaucophanites. e) S2 mylonitic foliation in Jd-bearing glaucophanites. f) D3 folding of S2 foliation in Jd-bearing glaucophanites and development of a discontinuous S3 foliation. g) Coronitic relict domains in metagabbros, wrapped by S2. h) Relict magmatic layering in poorly deformed metagabbros.

199x304mm (150 x 150 DPI)

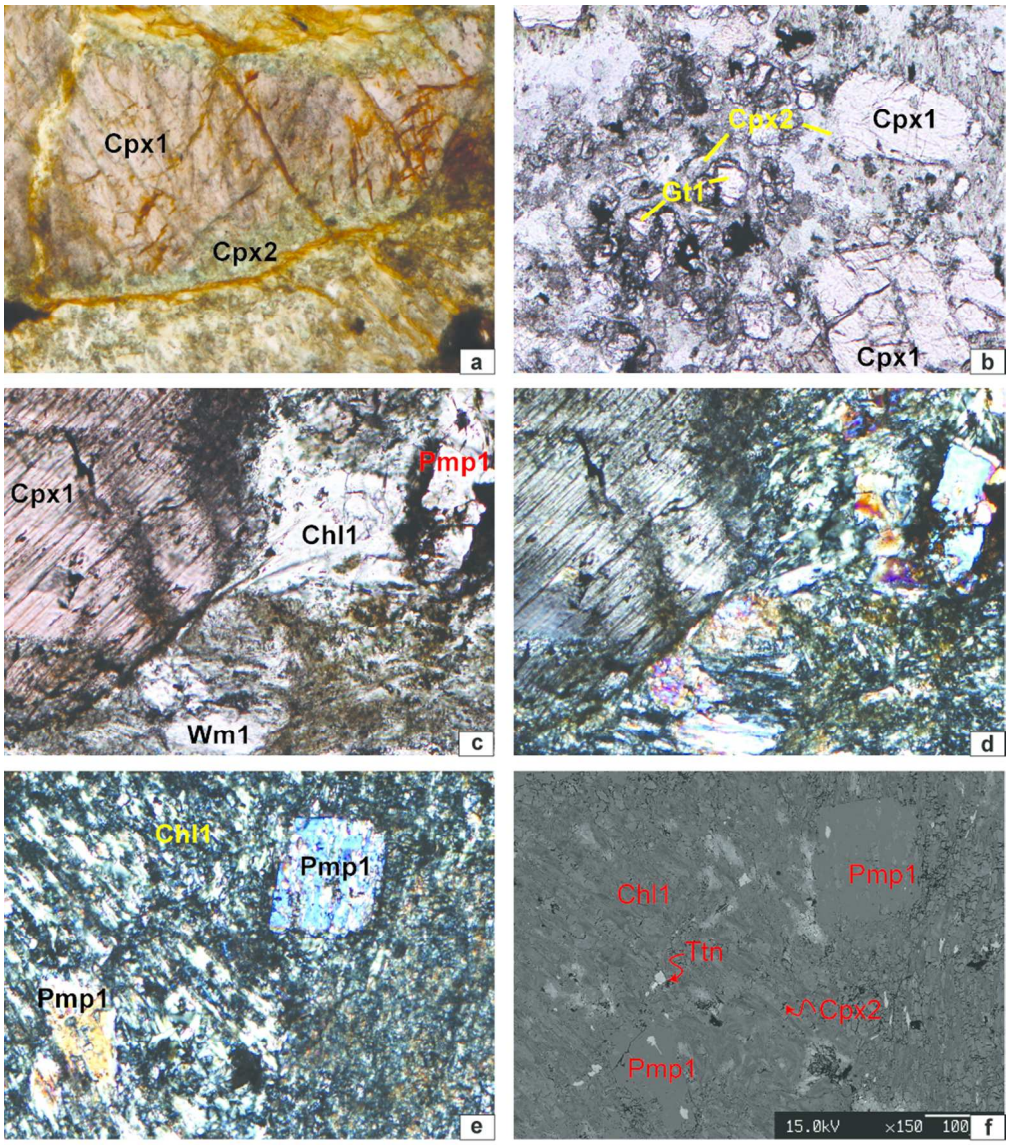

Figure 5: Microstructures in metagabbros. a) Cpx2 occurring as Cpx1 coronas; long side of photomicrograph (LSP) 0.86 mm. b) Cpx1 rimmed by Cpx2 and ex-Pl site replaced by Grt1 and Cpx2; LSP 0.86 mm. c) Interstitial ex-Pl sites between Cpx1 porphyroclasts replaced by Pmp1+Chl1 and Wm1+Chl1; LSP 0.86 mm. d) Crossed polar image of Fig. 5c; LSP 0.86 mm. e) Relicts of Cpx2 (see 4f) within Pmp1 and Chl1 sites; LSP 0.86 mm. f) Back-Scattered Electron (BSE) image of squared area located on Fig. 5e.

184x209mm (150 x 150 DPI)

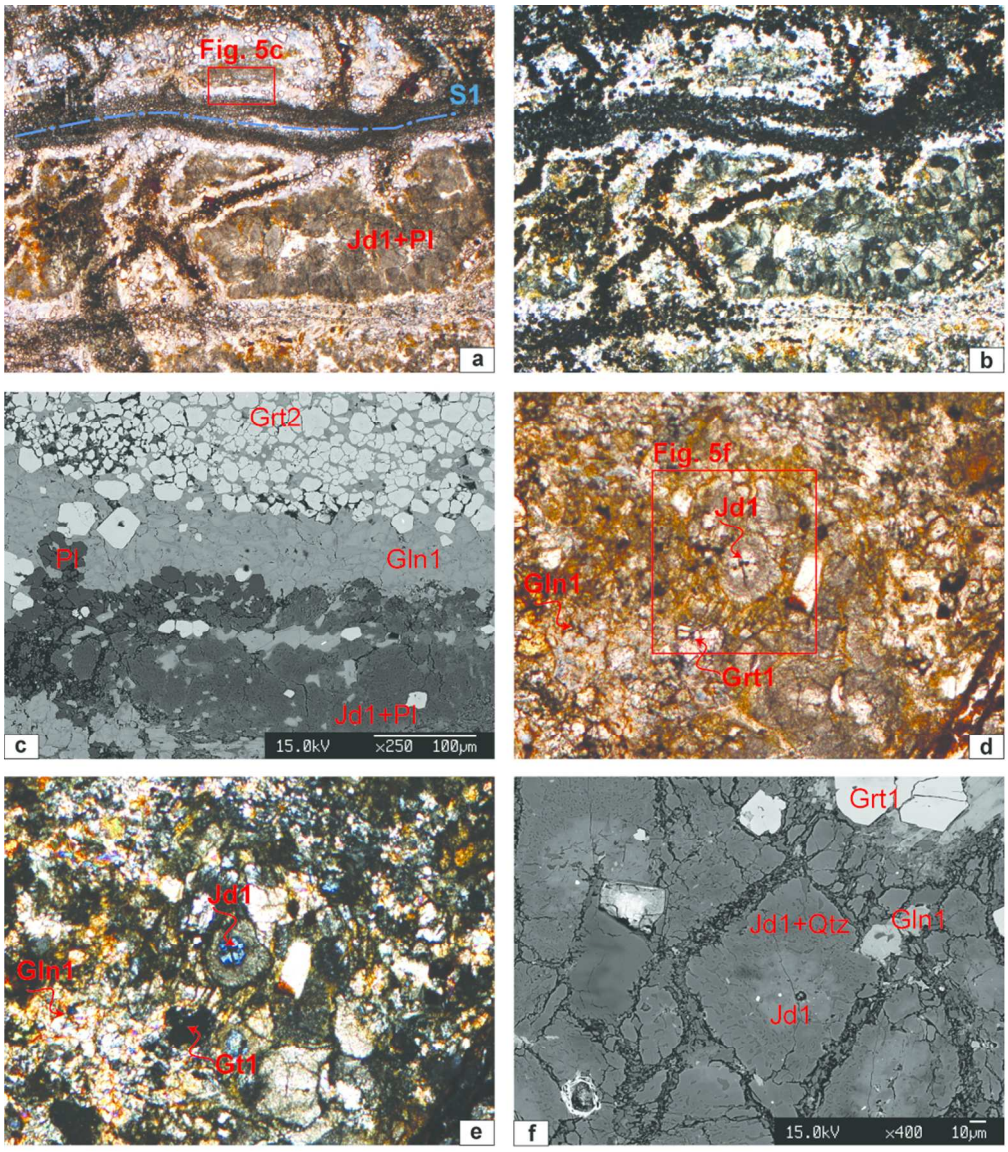

Figure 6: Microstructures in Jd-bearing glaucophanites. a) S1 foliation marked by elongated Jd-rich domains alternating with Gln1 and Grt2-rich layers; LSP 3.30 mm. b) Crossed polar image of Fig. 6a; LSP 3.30 mm. c) BSE image of squared area in Fig. 6c. d) Jd1 partially replaced by Gln1; LSP 0.86 mm. e) Crossed polar image of Fig. 6d to highlight blue interference colour for Jd-cores; LSP 0.86 mm. f) BSE image of squared area of Fig. 6d.

184x210mm (150 x 150 DPI)

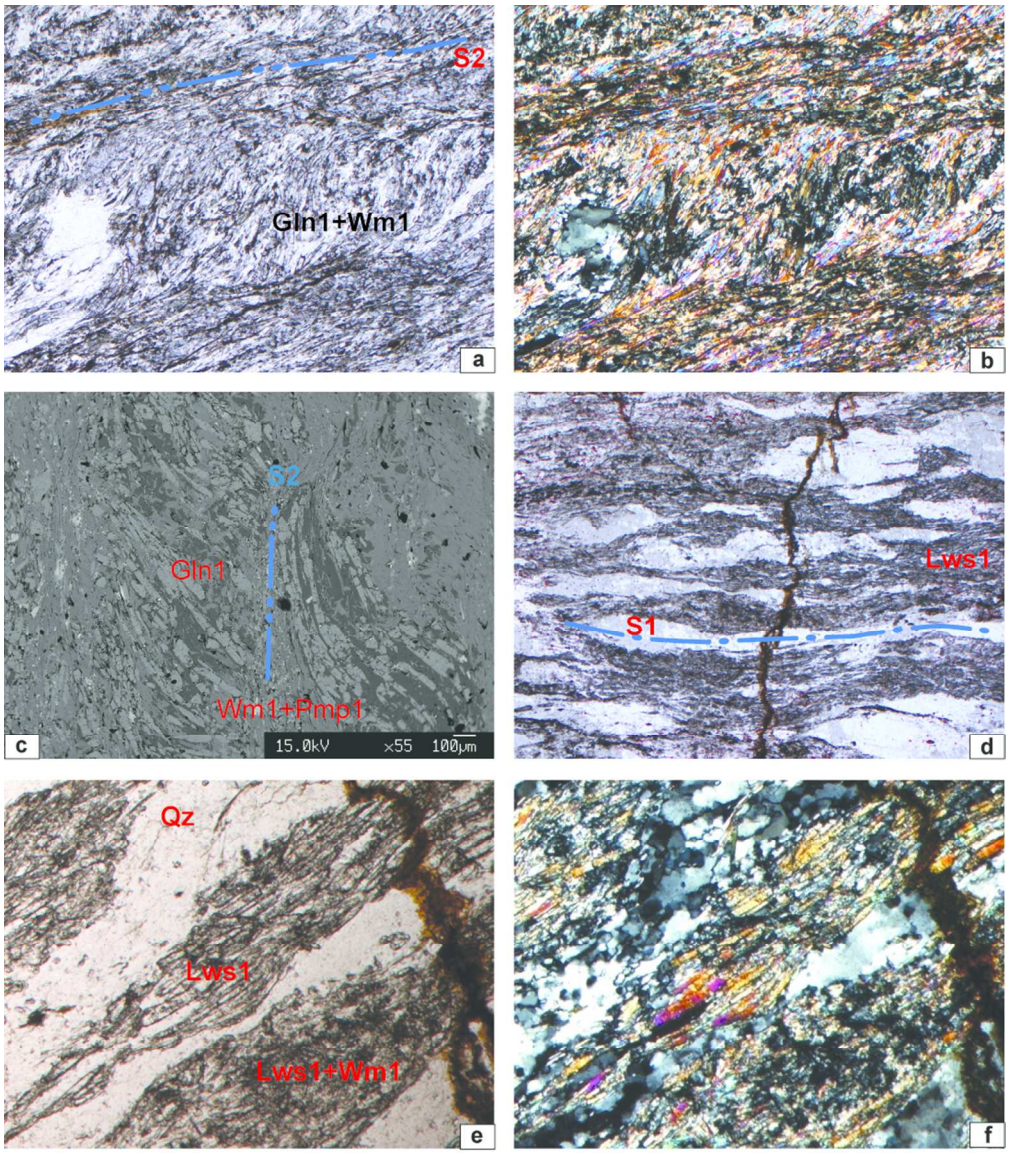

Figure 7: Microstructures in Lws-bearing glaucophanites. a) S2 films marked by Gln2+Wm1 and lithons hosting S1 foliation marked by Gnl1, Wm1 and Lws1; LSP 3.30 mm. b) Crossed polar image of Fig. 7a; LSP 3.30 mm. c) BSE image showing S2 foliation underlined by Wm1 and Pmp1 and S1 relict fabric marked by Gln1. d) S1 foliation marked by Lws1 and Wm1 SPO; LSP 3.30 mm. e) S1 foliation marked by Lws1 and Wm1 SPO; LSP 0.86 mm. f) Crossed polar image of Fig. 7e; LSP 0.86 mm.

184x211mm (150 x 150 DPI)

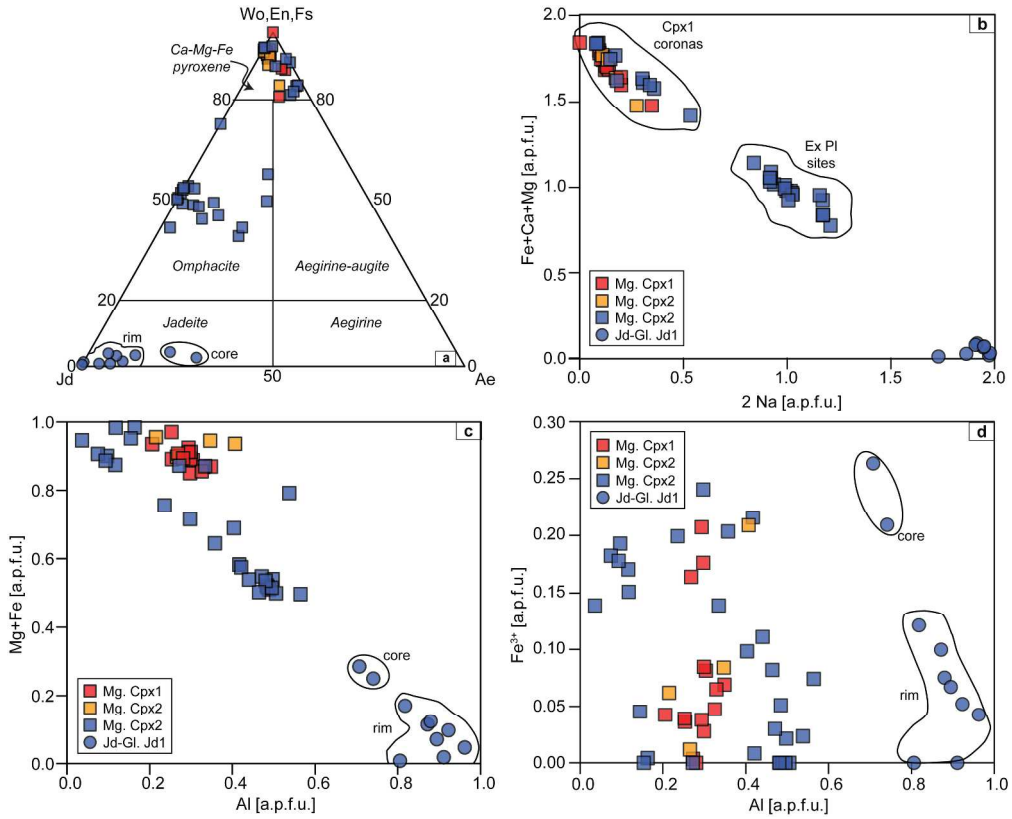

Figure 8: Compositional variations of Px in metagabbros and Jd-bearing glaucophanites. Cpx1 has diopside composition, whereas Cpx2 shows different composition as a function of the microstructural site: Cpx2 coronas on Cpx1 is diopside while Cpx2 replacing ex-Pl sites is omphacite. Jd1 has composition variable from core to rim. Legend: red squares = Cpx1 porphyroclasts in metagabbros (Mg); orange squares = Cpx2 exolutions in Cpx1 porphyroclasts in metagabbros; blue squares = Cpx2 in metagabbros; blue circles = Jd1 in Jd-bearing glaucophanites (Jd-Gl).

252x204mm (300 x 300 DPI)

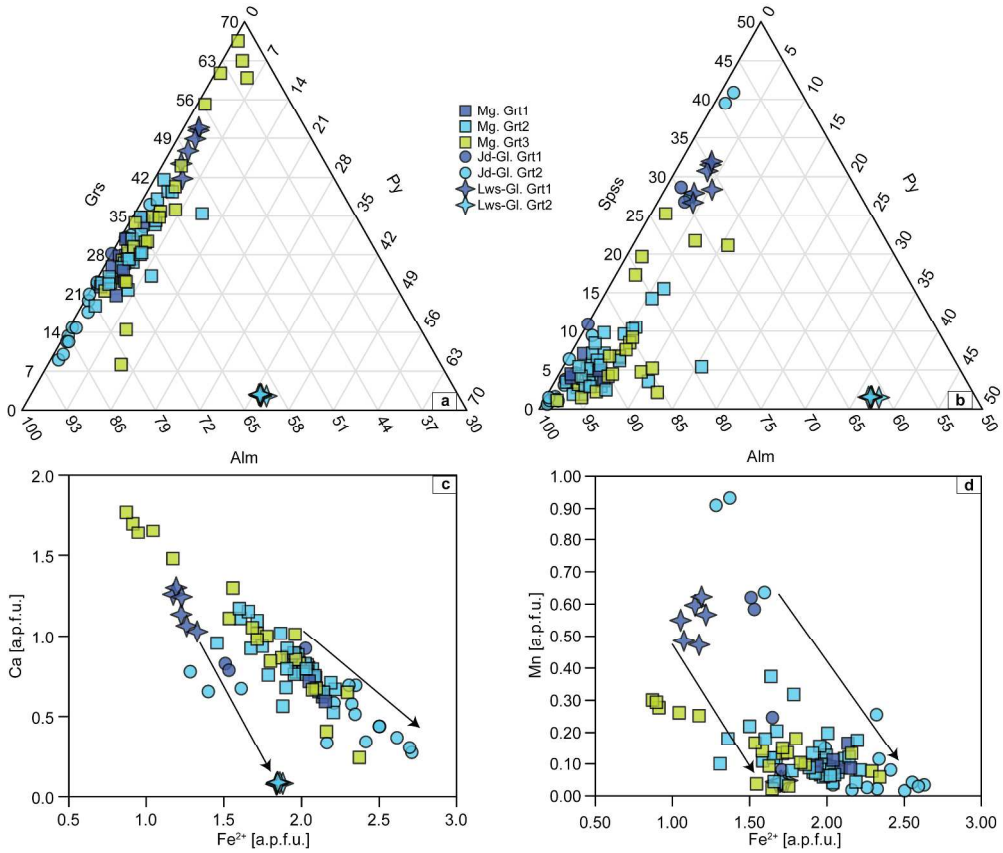

Figure 9: Compositional variation of Grt in all rocks. See text for details in compositional variations. Scale along axes in panels a and b may be different from 0-100%

262x221mm (300 x 300 DPI)

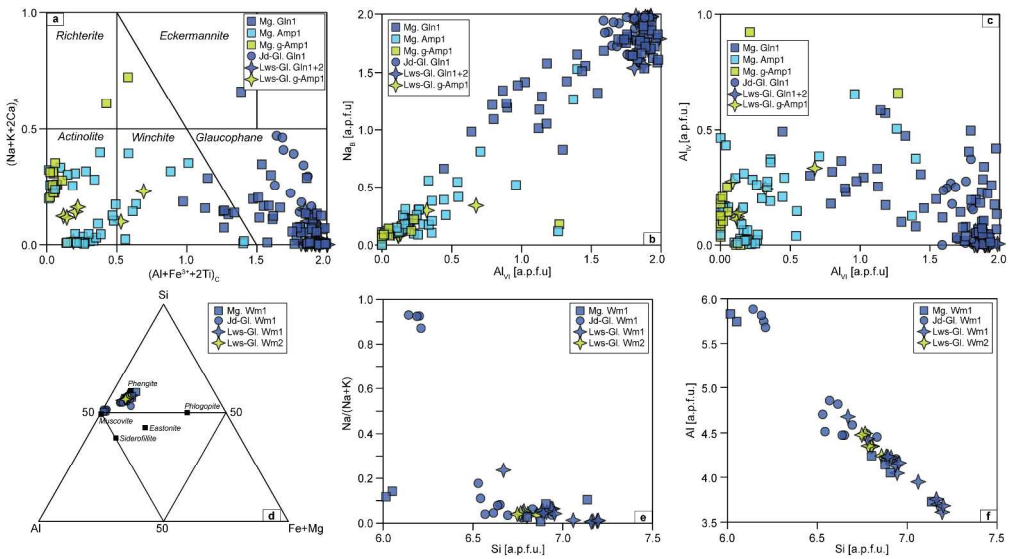

Figure 10: Compositional variation of Amp (a, b and c) and Wm (d, e and f) in the RCT metabasites. Amphiboles range between glaucophane to actinolite. White micas range from phengite to muscovite. Some high paragonite content is detected for micas from Jd-bearing glaucophanites.

374x205mm (300 x 300 DPI)

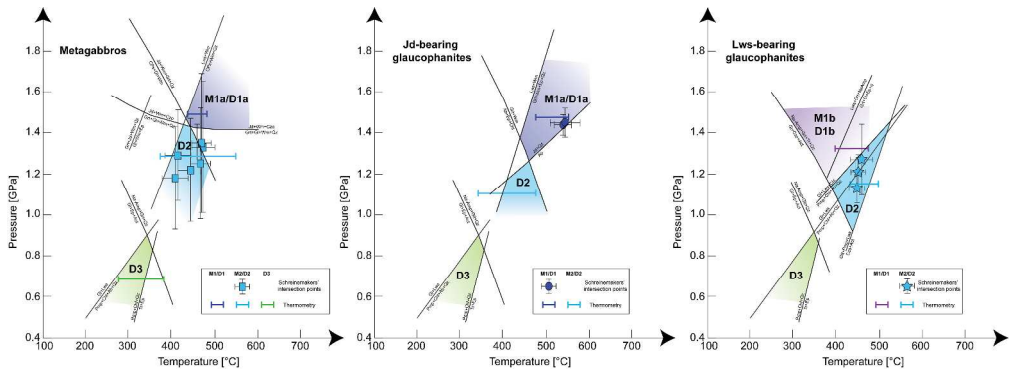

Figure 11: PT conditions for the three lithologies inferred from the integration of thermo-barometers, comparison of natural assemblages with experimental univariant equilibria, calculated reaction curves and stable intersections.

1573x566mm (150 x 150 DPI)

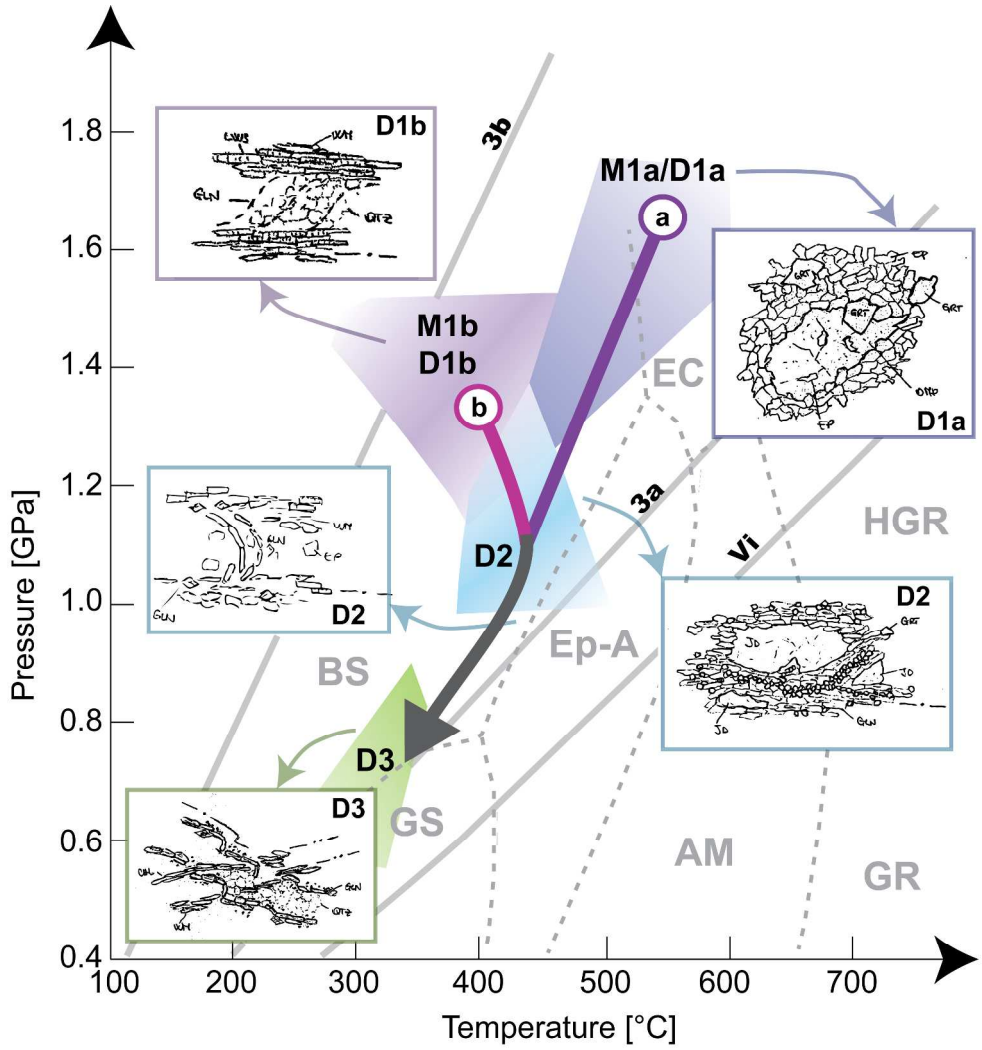

Figure 12: P-T-d history inferred from PT-estimates. In the insets the representation of dominant fabric and mineral assemblage for each stage is shown. Metamor- phic facies after (Ernst & Liou, 2008): GS=greenschist; Ep-A=epidote-bearing amphi- bolite; BS=blueschists; AM=amphibolite; EC=eclogite; HGR=high pressure granulite; GR=granulite. Geotherms: Vi=stable geotherms (England & Thompson, 1984) for continental crust; 3a) warm subduction zones, 3b) cold subduction zones (Cloos, 1993).

544x567mm (150 x 150 DPI)

Supporting Information for "Structural and metamorphic evolution of a subduction-related mélange: the example of Rocca Canavese Thrust Sheet (Italian Western Alps)"

Contents of this file

1. Tables 1 to 3: Details on compositional variations in minerals marking different metamorphic stages of (1) metagabbros, (2) Jd-bearing glaucophanites and (3) Lws-bearing glaucophanites.

Table 1: Details on compositional variations in minerals marking different metamorphic stages of metagabbros.

Mineral	M0	D1a	D2	D3
Cpx	Na=0.00-0.17	Na=0.04-0.60		
	Ca=0.80-0.95	Ca=0.07-0.96		
	Fe^{3+}=0.00-0.21	Fe^{3+}=0.00-0.24		
	Al_{tot}=0.21-0.35	Al_{tot}=0.04-0.56		
Amp			Na_B=0.66-1.90	Na_B=0.00-1.53
			Al_C=0.44-3.05	Al_C=0.00-1.91
			Ca_B=0.08-1.17	Ca_B=0.41-2.00
Gt		Ca=0.59-0.87	Ca=0.53-1.17	Ca=0.24-1.77
		Mg=0.03-0.13	Mg=0.03-0.23	Mg=0.02-0.34
		Fe=1.92-2.15	Fe=1.60-2.22	Fe=0.87-2.27
		Mn=0.09-0.17	Mn=0.04-0.37	Mn=0.02-0.30
Wm			Si=6.06-6.45	
			Ti=0.01-0.06	
			Al_{tot}=4.98-5.70	
			Mg=0.08-0.37	
			Pg=0.00-0.25	
Pl				Ca=0.00-0.01
				Na=0.97-1.01
				K=0.00-0.00
Ep				Al_{tot}=2.29-3.04
				Fe^{3+}=0.00-0.64
				Mn=0.00-0.02
Chl				Fe=1.95-5.00
				Mg=3.93-7.53
				Al=4.29-5.09
Pmp				Mg=0.29-0.39
				Fe=0.15-0.25

Table 2: Details on compositional variations in minerals marking different metamorphic stages of Jd-bearing glaucophanites.

Mineral	D1a	D2	D3
Cpx	Na=0.86-1.05		
	Ca=0.00-0.05		
	Fe^{3+}=0.00-0.26		
	Al_{tot}=0.71-0.96		
Amp		Na_B=1.65-1.97	
		Al_C=1.59-1.94	
		Ca_B=0.03-0.35	
Gt	Ca=0.78-0.92	Ca=0.27-0.78	
	Mg=0.00-0.07	Mg=0.00-0.08	
	Fe=1.53-2.03	Fe=1.28-2.71	
	Mn=0.08-0.62	Mn=0.02-0.93	
Wm	Si=6.14-6.94		
	Ti=0.00-0.02		
	Al_{tot}=4.21-5.88		
	Mg=0.02-0.68		
	Pg=0.02-0.93		
Pl		Ca=0.00-0.01	
		Na=0.97-1.01	
		K=0.00-0.00	
Ep		Al_{tot}=2.36-2.46	
		Fe^{3+}=0.45-0.61	
		Mn=0.01-0.02	
Chl			Fe=3.95-4.65
			Mg=2.79-3.03
			Al=4.89-5.08

Table 3: Details on compositional variations in minerals marking different metamorphic stages of Lws-bearing glaucophanites.

Mineral	D1b	D2	D3
Amp	Na_B=1.54-1.98		
	Al_C=1.81-1.99		
	Ca_B=0.01-0.22		
Gt	Ca=1.03-1.30	Ca=0.08-0.09	
	Mg=0.06-0.11	Mg=1.09-1.14	
	Fe=1.17-1.33	Fe=1.84-1.88	
	Mn=0.47-0.62	Mn=0.04-0.05	
Wm	Si=6.67-7.20		Si=6.75-6.86
	Ti=0.00-0.03		Ti=0.01-0.01
	Al_{tot}=3.62-4.68		Al_{tot}=4.24-4.49
	Mg=0.42-0.95		Mg=0.56-0.63
	Pg=0.01-0.24		Pg=0.03-0.05
Lws	Al=1.97-2.04		
	Fe_{tot}=0.01-0.03		
	Ca=0.91-0.94		
Pl		Ca=0.00-0.02	
		Na=0.98-1.01	
		K=0.00-0.03	
Ep		Al_{tot}=2.18-2.32	
		Fe^{3+}=0.70-0.86	
		Mn=0.01-0.02	
Pmp		Mg=0.42-0.51	
		Fe=0.12-0.14	
Chl			Fe=4.39-4.80
			Mg=4.52-5.00
			Al=4.59-5.11